

## From 0D dimer to 2D Network—Supramolecular Assembly of Organic Derivatized Polyoxometalates with Remote Hydroxyl via Hydrogen Bonding

Longsheng Wang,<sup>†</sup> Li Zhu,<sup>†,‡</sup> Panchao Yin,<sup>†</sup> Weiwei Fu,<sup>§</sup> Jiake Chen,<sup>†</sup> Jian Hao,<sup>†</sup> Fengping Xiao,<sup>†</sup> Chunlin Lv,<sup>†</sup> Jin Zhang,<sup>†</sup> Lu Shi,<sup>†</sup> Qiang Li,<sup>†</sup> and Yongge Wei<sup>\*†</sup>

<sup>†</sup>Department of Chemistry, Tsinghua University, Beijing 100084, China, <sup>‡</sup>Department of Chemistry and Chemical Engineering, Hunan University of Science and Technology, Xiangtan 4111201, China, and <sup>§</sup>School of Material and Science Technology, University of Science and Technology Beijing, Beijing 100083, China

Received May 19, 2009

A series of remote hydroxyl functionalized organoimido derivatives of hexamolybdate,  $(\text{Bu}_4\text{N})_2[\text{Mo}_6\text{O}_{18}(\text{Cres})]$  (**1**) (Cres = 4-amino-*m*-cresol),  $(\text{Bu}_4\text{N})_2[\text{Mo}_6\text{O}_{17}(\text{Cres})_2] \cdot \text{H}_2\text{O}$  (**2**),  $(\text{Bu}_4\text{N})_2[\text{Mo}_6\text{O}_{18}(\text{Phen})] \cdot i\text{-PrOH}$  (Phen = *p*-aminophenol) (**3**),  $(\text{Bu}_4\text{N})_2[\text{Mo}_6\text{O}_{18}(\text{Phen})] \cdot \text{EtOH}$  (**4**),  $(\text{Bu}_4\text{N})_2[\text{Mo}_6\text{O}_{17}(\text{Phen})_2]$  (**5**),  $(\text{Bu}_4\text{N})_2[\text{Mo}_6\text{O}_{18}(\text{Naph})]$  (Naph = 5-amino-1-naphthyl) (**6**), and  $(\text{Bu}_4\text{N})_2[\text{Mo}_6\text{O}_{18}(\text{Chex})] \cdot 1.5\text{H}_2\text{O}$  (Chex = *trans*-4-aminocyclohexanol) (**7**) were synthesized and characterized by single crystal X-ray diffraction, FT-IR spectra, UV–vis spectra, elemental analysis, <sup>1</sup>H NMR, and cyclic voltammetry. X-ray structural study reveals that intermolecular and intramolecular hydrogen bonding plays an important role in their supramolecular assembly; it is found that (i) bridged oxo ligands of hexamolybdate cluster are more inclined to form hydrogen bonds as acceptors than terminal oxo ligands in this system; (ii) small solvent molecules with hydrogen bonding donor and acceptor, such as water, *i*-PrOH, and EtOH, usually act as hydrogen bonding bridge in their supramolecular assembly; (iii) hydrogen bonding has an important influence on their anion conformation besides cell packing; (iv) the hydrogen bonding supramolecular assembly of compounds **1–7** demonstrate an interesting change from dimer (**3**), to 1D infinite single chain (**4**), to 1D infinite double chain (**2**), and to 2D network (**1**, **5**, **6**, and **7**) owing to the alteration of the grafting organic ligand, the substituted number, and the crystallized solvent molecule. To explore their potential application in conductivity, the optical band gap of compounds **1–7** were determined upon their solid state reflectance spectra. Our current study not only surveys systematically hydrogen bonding interaction and supramolecular assembly of remote hydroxyl functionalized organoimido-derivatized hexamolybdates but also provides some available precursors for further modification including esterification.

### Introduction

In the past century, the research on supramolecular chemistry had an explosive breakthrough along with increasing knowledge on intermolecular noncovalent interactions, such as hydrogen bonding,  $\pi \cdots \pi$  interaction, dipole  $\cdots$  dipole interaction, and van der Waals interactions.<sup>1</sup> The hydrogen bond, as one type of ubiquitous noncovalent interaction, plays a significant role in molecular recognition and crystal engineering owing to its unique bond intensity and directionality. To date, great advances have been made in organic solid science by using hydrogen bonding as a bridge and proper hydrogen synthons as a nexus, and a number of hydrogen-bonded rosettes, capsules, spheres, dendrimers, polymers,

and other architectures have been designed and achieved through selection of the proper hydrogen bond donor and acceptor.<sup>2</sup> Currently, crystal engineering utilizing hydrogen bonding synthons containing a functional inorganic cluster is drawing more and more researchers' attentions because it affords a rational and reproducible route to design and construct functional supramolecular materials containing luminescent, electronic, or magnetic units.<sup>3</sup>

\*To whom correspondence should be addressed. E-mail: yonggewei@tsinghua.edu.cn. Phone: +86-10-62797852. Fax: +86-10-62757497.

(1) (a) Desiraju, G. R. *Acc. Chem. Res.* **1996**, *29*, 441. (b) Behr, J.-P. *The Lock and Key Principle. The State of the Art –100 Years on. Perspectives in Supramolecular Chemistry*; Wiley: Chichester, 1995; Vol. 1; (c) Sharma, C. V. K.; Desiraju, G. R., *Perspectives in Supramolecular Chemistry. The Crystal as a Supramolecular Entity*; Wiley: Chichester, 1996; (d) Mingos, D. M. P., *Supramolecular Assembly via Hydrogen Bonds II. Structure and Bonding*; Springer-Verlag: New York, 2005; (e) Lehn, J. M., *Supramolecular Chemistry*; VCH: Weinheim, 1995.

(2) (a) Ikkala, O.; Brinke, G. T. *Science* **2002**, *295*, 2407. (b) Zeng, F.-w.; Zimmerman, S. C. *Chem. Rev.* **1997**, *97*, 1681. (c) Morgan, C. M.; Rebek, J. J. *Chem. Rev.* **1997**, *97*, 1647. (d) Chichak, K. S.; Cantrill, S. J.; Pease, A. R.; Chiu, S.-H.; Cave, G. W. V.; Atwood, J. L.; Stoddart, J. F. *Science* **2004**, *295*, 2407. (e) McKinlay, R. M.; Thallapally, P. K.; Cave, G. W. V.; Atwood, J. L. *Angew. Chem., Int. Ed.* **2005**, *44*, 5733.

(3) (a) Braga, D.; Grepioni, F.; Desiraju, G. R. *Chem. Rev.* **1998**, *98*, 1375. (b) Cotton, F. A.; Lin, C.; Murillo, C. A. *Acc. Chem. Res.* **2001**, *34*, 759. (c) Blake, A. J.; Champness, N. R.; Hubberstey, P.; Li, W.-S.; Withersby, M. A.; Schröder, M. *Coord. Chem. Rev.* **1999**, *183*, 117. (d) Burkhardt, A.; Spielberg, E. T.; Simon, S.; Gorls, H.; Buchholz, A.; Plass, W. *Chem.—Eur. J.* **2009**, *15*, 1261. (e) Adachi, K.; Sugiyama, Y.; Yoneda, K.; Yamada, K.; Nozaki, K.; Fuyuhiko, A.; Kawata, S. *Chem.—Eur. J.* **2005**, *11*, 6616. (f) Zhou, W.; Li, D. J. B.; He, X. R.; Li, C. H.; Lv, J.; Li, Y. L.; Wang, S.; Liu, H. B.; Zhu, D. B. *Chem.—Eur. J.* **2008**, *14*, 754.

Polyoxometalates (POMs) are a vast class of discrete anion clusters consisting of early transition metal ions (such as molybdenum, tungsten, vanadium, niobium, and tantalum) in their higher oxidation state and oxo ligand. POMs chemistry has drawn growing research interest from different fields since the discovery of  $[\text{PMo}_{12}\text{O}_{40}]^{3-}$  by Berzelius in 1826. That is not only owing to their diverse structures with low to high nuclearity ranging from 5 to 368 metal atoms in a single molecule but also because of their potential applications in diverse fields including electrochemistry, catalysis, magnetism, medicine, photochemistry, and semiconductor molecular materials.<sup>4</sup> In the tide of supramolecular chemistry, supramolecular POMs also have drawn increasing attention. The strategy using POM clusters as building blocks to construct supramolecular architectures has made considerable advances up to now. Müller reported that the pores of a nanoscale giant POM capsule could be gated by cations of  $\text{Pr}^{3+}$  depending on the change of concentrations of  $\text{Pr}^{3+}$ ,<sup>5</sup> Hill et al. demonstrated a catalytic 2D coordination network composed of  $[\text{V}_6\text{O}_{13}\{(\text{OCH}_2)_3\text{C}(\text{NHCH}_2\text{C}_6\text{H}_4-4\text{-CO}_2)\}_2]^{4-}$  and  $\text{Tb}(\text{III})$ ,<sup>6</sup> Wang et al. recently reported a chiral 3D architecture with helical channels constructed by  $[\text{BW}_{12}\text{O}_{40}]^{5-}$  and a copper/amino acid building block,<sup>7</sup> Yang et al. reported a series of robust POM–organic frameworks (POMOFs) using lacunary Keggin as secondary building unit (SBU),<sup>8</sup> and a class of supramolecular molecular materials with semiconductivity has been built up using POM clusters and organic  $\pi$ -electron donor ligands by Coronado group.<sup>9</sup> One exciting discovery by Liu is that nanoscale giant POM clusters were assembled into hollow vesicle structures, which could be observed by static laser scattering (SLS) and dynamic laser scattering (DLS) techniques.<sup>10</sup>

However, few efforts were devoted to the research of intermolecular noncovalent interactions in POM systems, even of hydrogen bonding, which has been found to play an important role in the pseudo liquid structure of POMs.<sup>11</sup> We are still short of enough knowledge to realize the crystal engineering of POMs. For instance, it is difficult to estimate whether a bridged oxo ligand or a terminal oxo ligand is more inclined to form hydrogen bonds in the presence of an

appropriate hydrogen bonding donor owing to the high symmetry of POM anion clusters.<sup>12</sup> Additionally, there are many crystallized water molecules in the cell unit of those common or giant POMs; it is still a great challenge to analyze and describe their hydrogen bonding interactions because there are so many hydrogen bonds and some possible position disorder of the crystal water molecules in those compounds.<sup>13</sup> The functionalization of POMs by an organic ligand to reduce the symmetry of POMs clusters and using organic anions to lessen the influence of crystal water may be an effective strategy to study the noncovalent interaction of POMs and provides a more rational approach toward supramolecular POMs.

As one important branch of POM chemistry, functionalization of POMs using organic ligands or organometallic units has been expanding rapidly over the past three decades because the modification of POMs provides one rational and designable approach toward POMs with tunable structures and properties.<sup>14</sup> Up to now, the POMs clusters, such as Lindqvist, Keggin, Dawson, and lacunary Keggin or Dawson polyanion, had been extensively modified by various organic ligands or organometallic units, including organosilica, organotin, alkyloxo, organoimido, and nitrosyl.<sup>14</sup> Especially, aryimido derivatives of POMs have drawn many research interests recently owing to the so-called “synergistic interaction” between the inorganic POM cluster and the organic ligand.<sup>15a</sup> On the other hand, the adaptability of imido derivatives renders them able to bear many kinds of remote functional groups, such as halogen,  $-\text{CN}$ ,  $-\text{C}\equiv\text{CH}$ ,  $-\text{CH}=\text{CH}_2$ .<sup>15–19,22–26</sup> Those derivatives with proper remote

(4) (a) *Polyoxometalates Chemistry: From Topology Via Self-Assembly to Applications*; Pope, M. T., Müller, A., Eds.; Kluwer: Dordrecht, 2001. (b) Pope, M. T.; Müller, A. *Angew. Chem., Int. Ed. Engl.* **1991**, *30*, 34. (c) Moffat, J. B. *Metal–Oxygen Clusters—The Surface and Catalytic Properties of Heteropoly Oxometalates*; Kluwer Academic Publishers: Norwell, MA, 2002. (d) An excellent review on the present status of the field of POMs is given in articles by leading experts in: *Chem. Rev.* **1998**, *98*, 1–387. (e) Pope, M. T. *Heteropoly and Isopoly Oxometalates*; Springer: Berlin, 1983; (f) Long, D. L.; Burkholder, E.; Cronin, L. *Chem. Soc. Rev.* **2007**, *36*, 105.

(5) Müller, A.; Zhou, Y. S.; Bogge, H.; Schmidtman, M.; Mitra, T.; Haupt, E. T. K.; Berkle, A. *Angew. Chem., Int. Ed.* **2006**, *45*, 460.

(6) Han, J. W.; Hill, C. L. *J. Am. Chem. Soc.* **2007**, *129*, 15094.

(7) An, H. Y.; Wang, E. B.; Xiao, D. R.; Li, Y. G.; Su, Z. M.; Xu, L. *Angew. Chem., Int. Ed.* **2006**, *45*, 904.

(8) Zheng, S. T.; Zhang, H.; Yang, G. Y. *Angew. Chem., Int. Ed.* **2008**, *47*, 3909.

(9) (a) Coronado, E.; Gomez-Garcia, C. J. *Chem. Rev.* **1998**, *98*, 273. (b) Coronado, E.; Galan-Mascaros, J. R.; Gimenez-Saiz, C.; Gomez-Garcia, C. J.; Triki, S. J. *Am. Chem. Soc.* **1998**, *120*, 4671.

(10) Liu, T. B.; Diemann, E.; Li, H. L.; Dress, A. W. M.; Müller, A. *Nature* **2003**, *426*, 59.

(11) Kozhevnikov, I. V. *Catalysis by Polyoxometalates*; John Wiley & Sons: New York, 2002; Vol. 2.

(12) (a) Zheng, P.-Q.; Ren, Y.-P.; Long, L.-S.; Huang, R.-B.; Zheng, L.-S. *Inorg. Chem.* **2005**, *44*, 1190. (b) Han, Z. G.; Zhao, Y. L.; Peng, J.; Ma, H. Y.; Liu, Q.; Wang, E. B.; Hu, N. H. *J. Solid State Chem.* **2004**, *177*, 4325. (c) Duan, W.-J.; Cui, X.-B.; Xu, Y.; Xu, J.-Q.; Yu, H.-H.; Yi, Z.-H.; Cui, J.-W.; Wang, T.-G. *J. Solid State Chem.* **2007**, *180*, 1875.

(13) (a) Müller, A.; Krickemeyer, E.; Bogge, H.; Schmidtman, M.; Beugholt, C.; Kogerler, P.; Lu, C. Z. *Angew. Chem., Int. Ed.* **1998**, *37*, 1220. (b) Evans, H. T., Jr. In *Polyoxometalates: From Platonic Solids to Anti-Retroviral Activity*; Pope, M. T., Müller, A., Eds.; Kluwer Academic Publishers: Dordrecht, 1994; p 71.

(14) (a) Proust, A.; Thouvenot, R.; Gouzerh, P. *Chem. Commun.* **2008**, No. 16, 1837. (b) Gouzerh, P.; Proust, A. *Chem. Rev.* **1998**, *98*(1), 77.

(c) Errington, R., In *Polyoxometalates Chemistry: From Topology Via Self-Assembly to Applications*; Pope, M. T., Müller, A., Eds.; Kluwer Academic Publishers: Dordrecht, 2002; pp 7–22. (d) Moore, A. R.; Kwen, H.; Hamaker, C. G.; Mohs, T. R.; Beatty, A. M.; Harmon, B.; Needham, K.; Maatta, E. A. In *Polyoxometalate Chemistry for Nano-Composite Design*; Yamase, T., Pope, M. T., Eds.; Kluwer Academic: New York, 2002; pp 129–138.

(15) (a) Peng, Z. *Angew. Chem., Int. Ed.* **2004**, *43*, 930. (b) Kwen, H.; Beatty, A. M.; Maatta, E. A. C. R. *Chim.* **2005**, *8*, 1025.

(16) (a) Xia, Y.; Wu, P.; Wei, Y.; Wang, Y.; Guo, H. *Cryst. Growth Des.* **2006**, *6*, 253. (b) Xue, S.; Xiang, C.; Wei, Y.; Tao, Z.; Chai, A.; Bian, W.; Xu, Z. *Cryst. Growth Des.* **2008**, *8*, 2437. (c) Zhu, Y.; Xiao, Z.; Ge, N.; Wang, N.; Wei, Y.; Wang, Y. *Cryst. Growth Des.* **2006**, *6*, 1620.

(17) (a) Xu, B.; Lu, M.; Kang, J.; Wang, D.; Brown, J.; Peng, Z. *Chem. Mater.* **2005**, *17*, 2841. (b) Lu, M.; Xie, B.; Kang, J.; Chen, F.-C.; Yang, Y.; Peng, Z. *Chem. Mater.* **2005**, *17*, 402. (c) Moore, A. R.; Kwen, H.; Beatty, A. M.; Maatta, E. A. *Chem. Commun.* **2000**, 1793.

(18) Kang, J.; Xu, B.; Peng, Z.; Zhu, X.; Wei, Y.; Powell, D. R. *Angew. Chem., Int. Ed.* **2005**, *44*, 6902.

(19) (a) Wei, Y.; Xu, B.; Barnes, C. L.; Peng, Z. *J. Am. Chem. Soc.* **2001**, *123*, 4083. (b) Hao, J.; Ruhlmann, L.; Zhu, Y.; Li, Q.; Wei, Y. *Inorg. Chem.* **2007**, *46*, 4960. (20) Song, Y. F.; Long, D. L.; Cronin, L. *Angew. Chem., Int. Ed.* **2007**, *46*, 3900.

(21) Clegg, W.; Errington, R. J.; Fraser, K. A.; Holmes, S. A.; Schaefer, A. J. *Chem. Soc., Chem. Commun.* **1995**, 455.

(22) Pradeep, C. P.; Long, D. L.; Newton, G. N.; Song, Y. F.; Cronin, L. *Angew. Chem., Int. Ed.* **2008**, *47*, 4388.

(23) Hao, J.; Xia, Y.; Wang, L.; Ruhlmann, L.; Zhu, Y.; Li, Q.; Yin, P.; Wei, Y.; Guo, H. *Angew. Chem., Int. Ed.* **2008**, *47*, 2626.

(24) Strong, J. B.; Yap, G. P. A.; Ostrander, R.; Liable-Sands, L. M.; Rheingold, A. L.; Thouvenot, R.; Gouzerh, P.; Maatta, E. A. *J. Am. Chem. Soc.* **2000**, *122*, 639.

(25) Wu, P.; Li, Q.; Ge, N.; Wei, Y.; Wang, Y.; Wang, P.; Guo, H. *Eur. J. Inorg. Chem.* **2004**, 2819.

(26) Xu, L.; Lu, M.; Xu, B.; Wei, Y.; Peng, Z.; Powell, D. R. *Angew. Chem., Int. Ed.* **2002**, *41*, 4129.

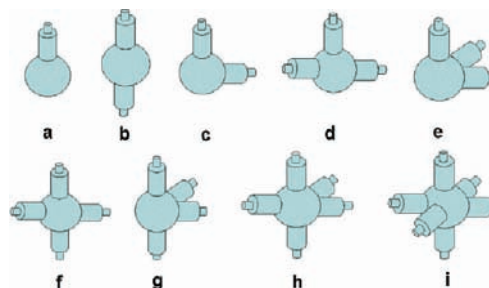
functional groups can be used not only as a monomer to construct organic–inorganic hybrid polymers through controlled organic reactions<sup>17</sup> but also as a metalloligand to construct supramolecular compounds by coordination reactions.<sup>18</sup> It has been found that weak noncovalent interactions (i.e., the C–H···O hydrogen bonding) play important roles in the cell packing of organic derivatized POMs.<sup>19a</sup> Cronin et al. recently reported one example of noncovalently connected frameworks with nanoscale channels assembled from a tethered Anderson-type POM–pyrene hybrid of  $[\text{TBA}]_3\text{-}[\text{MnMo}_6\text{O}_{18}\{(\text{OCH}_2)_3\text{CNHCH}_2\text{C}_{16}\text{H}_9\}_2]\cdot 2\text{DMF}\cdot 3\text{H}_2\text{O}$  using intermolecular C–H···O hydrogen bonding.<sup>20</sup> However, it is still a great challenge to construct supramolecular POMs utilizing the C–H···O hydrogen bonding because of the weak bond intensity and the directional nature of the C–H···O hydrogen bonding. Therefore, another strategy was adopted to introduce some strong hydrogen bonding donor functional groups such as  $\text{NH}_2$  or  $\text{OH}$  onto the POM skeleton to accomplish rational supramolecular assembly. Indeed, Errington et al. had reported one linear bifunctionalized derivative of hexamolybdates with a remote amine group.<sup>21</sup> Cronin recently reported one example of amino group functionalized Dawson POMs,  $[(\text{C}_{16}\text{H}_{36}\text{N})_{19}\{\text{H}_2\text{NC}(\text{CH}_2\text{O})_3\text{P}_2\text{V}_3\text{W}_{15}\text{O}_{59}\}_4]^{5-}$ , which form macromolecular hydrogen bonded nanoassemblies of POM clusters via intermolecular hydrogen bonding of  $\text{N}-\text{H}\cdots\text{O}$ .<sup>22</sup>

To investigate the hydrogen bonding interaction and supramolecular assembly of POMs,  $[\text{Mo}_6\text{O}_{19}]^{2-}$ , the smallest POM cluster with high symmetry of  $O_h$ , was chosen as the parent cluster to be modified. Not only the six terminal oxo ligands but also the bridged oxo ligands of the hexamolybdate cluster could be substituted by an organoimido ligand to form monosubstituted to hexasubstituted imido derivatives containing different remote functional groups;<sup>23,24</sup> the organoimido derivatives of hexamolybdate have different molecular topology according to their different substituted extent and substituted mode (as shown in Scheme 1).<sup>24</sup> They will be excellent building blocks with well-defined topology if these attached organic ligands have a proper remote functional group. In this paper, four ligands of 4-amino-*m*-cresol (Cres), *p*-aminophenol (Phen), 5-amino-1-naphthyl (Naph), and *trans*-4-aminocyclohexanol (Chex) containing a remote hydroxyl functional group (as shown in Scheme 2) were selected for imidization, and five monofunctionalized and two bifunctionalized organoimido derivatives of hexamolybdate were obtained and structurally characterized. We herein report the synthesis, structures, characterizations, hydrogen bonding assemblies, and electrochemical studies of  $(\text{Bu}_4\text{N})_2[\text{Mo}_6\text{O}_{18}(\text{Cres})]$  (**1**),  $(\text{Bu}_4\text{N})_2[\text{Mo}_6\text{O}_{17}(\text{Cres})_2]\cdot\text{H}_2\text{O}$  (**2**),  $(\text{Bu}_4\text{N})_2[\text{Mo}_6\text{O}_{18}(\text{Phen})]\cdot i\text{-PrOH}$  (**3**),  $(\text{Bu}_4\text{N})_2[\text{Mo}_6\text{O}_{18}(\text{Phen})]\cdot\text{EtOH}$  (**4**),  $(\text{Bu}_4\text{N})_2[\text{Mo}_6\text{O}_{17}(\text{Phen})_2]$  (**5**),  $(\text{Bu}_4\text{N})_2[\text{Mo}_6\text{O}_{18}(\text{Naph})]$  (**6**), and  $(\text{Bu}_4\text{N})_2[\text{Mo}_6\text{O}_{18}(\text{Chex})]\cdot 1.5\text{H}_2\text{O}$  (**7**).

## Experimental Details

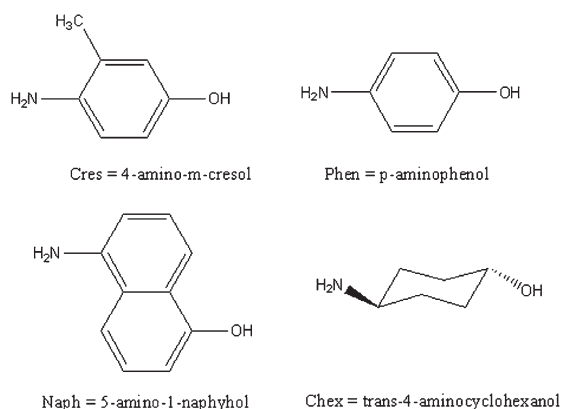
All synthesis and manipulations were performed using ordinary organic synthetic apparatuses and techniques.  $[\text{Bu}_4\text{N}]_4[\alpha\text{-Mo}_8\text{O}_{26}]$  was synthesized according to literature procedure<sup>37</sup> and confirmed by IR. All amine hydrochlorides were prepared by the addition of concentrated HCl to an aqueous solution of alkyl amines, from which the products were obtained by evaporating the solvent under vacuum. Other chemical reagents purchased were of analytical grade and used without further purification, except for acetonitrile,

**Scheme 1.** Schematic Diagrams for Different Substituted Extents and Substituted Modes of Lindqvist<sup>24</sup>



(a) Lollipop model for monofunctionalized; (b,c) linear and angle type for bifunctionalized; (d,e) “T” and triangle type for trifunctionalized; (f,g) “+” and “K” type for tetrafunctionalized; (h) pentafunctionalized; and (i) superoctahedron type for hexafunctionalized.

**Scheme 2.** Selected Four Kinds of Ligands Containing a Remote Hydroxyl for the Functionalization of POMs



which was dried by refluxing in the presence of  $\text{CaH}_2$  and distilled prior to use. Elemental analysis were performed on a (Elementar Analytensysteme GmbH) Vario EL. FT-IR spectra were measured using KBr pellets and recorded on a Perkin Elmer FT-IR spectrophotometer. UV–vis spectra were measured in acetonitrile solutions with an UV2100S Spectrophotometer (Shimadzu).  $^1\text{H}$  NMR spectra for compounds **2–6** were taken on a JEOL JNM-ECA300 NMR spectrometer at 300 K using  $\text{DMSO}-d_6$  as solvent (**1** using  $\text{CD}_3\text{CN}$  and **7** using  $\text{acetone}-d_6$ ). Optical diffuse reflectance spectra were performed on a Shimadzu UV-3100 recording spectrophotometer with  $\Phi$  60 mm integrating sphere from 240 to 2600 nm at room temperature. Initially, the 100% line flatness of the spectrophotometer was set using barium sulfate ( $\text{BaSO}_4$ ). A powder sample of the measured compound was mounted on the sample holder. The thickness of the sample was approximately 2.00 mm, which was much greater than the size of the individual crystal particles.<sup>36</sup>

**Electrochemical Experiments.** *N,N*-dimethylformamide (DMF) for cyclic voltammetry (CV) measurements was HPLC grade and used as received without purification. The sample concentration is about 1 mM. The solutions were deaerated thoroughly by bubbling high pure  $\text{N}_2$  through the solution for 15–20 min and kept under high pure  $\text{N}_2$  atmosphere during the whole experiment. The diameter of working Pt electrodes is 2 mm. The electrochemical apparatus CHI750A was driven by a personal computer. Potentials are quoted versus a saturated calomel electrode (SCE). The counter electrode was a platinum plate with a large surface area. All experiments were carried out at room temperature.  $[\text{Bu}_4\text{N}]\text{PF}_6$  was used as the supporting electrolyte, and a scan rate was  $50\text{ mV s}^{-1}$ .  $E_{\text{pa}}$  and  $E_{\text{pc}}$  values (vs SCE) were determined using a sigmoidal method provided by the program package of CHI750A,  $\Delta E_p = E_{\text{pa}} - E_{\text{pc}}$ ,  $E_{1/2} = (E_{\text{pa}} + E_{\text{pc}})/2$ .

**X-ray Crystallography.** Suitable crystals were mounted on glass fibers and transferred onto the diffractometer rapidly. X-ray diffraction data of **5** were collected on a Bruker Smart Apex CCD diffractometer using graphite-monochromatized Mo  $K_{\alpha}$  radiation ( $\lambda = 0.71073$  Å) at room temperature ( $293 \pm 2$  K). The X-ray diffraction data of **2**, **3**, **4**, **6**, and **7** were collected on a Rigaku RAXIS-SPIDER IP diffractometer using graphite-monochromatized Mo  $K_{\alpha}$  radiation ( $\lambda = 0.71073$  Å) at room temperature ( $293 \pm 2$  K). Data collections for compound **5** were using the SMART software. Data reduction, cell refinement, and experiential absorption correction for **5** were carried out using SAINT. Data collection and data reduction, cell refinement, and experiential absorption correction for compounds **2**, **3**, **4**, **6**, and **7** were performed with the software package of Rigaku RAPID AUTO (Rigaku, 1998, Ver2.30). Structures of all compounds were solved by direct methods and refined against  $F^2$  by full matrix least-squares. All non-hydrogen atoms, except disordered atoms, were refined anisotropically. Hydrogen atoms of all carbon atoms were generated geometrically. All calculations were performed using the program package of SHELXS-97.<sup>38</sup>

**Synthesis of Monofunctionalized Compounds. Method A.** A mixture of 1.0 mmol  $(\text{Bu}_4\text{N})_4[\alpha\text{-Mo}_8\text{O}_{26}]$  (2.15 g), 2.1 mmol  $N,N'$ -dicyclohexylcarbodiimide (DCC; 0.43 g) and 1.34 mmol hydrochloride salt of amine (0.21 g hydrochloride salt of 4-amino-*m*-cresol for **1**, 0.19 g hydrochloride salt of 4-amino-*m*-cresol for **3** and **4**, 0.27 g hydrochloride salt of 5-amino-1-naphenol for **6**, and 0.20 g hydrochloride salt of *trans*-4-aminocyclohexanol for **7**) was refluxed at  $100\text{--}110$  °C in 20 mL of anhydrous acetonitrile. After 6–12 h, the resulting black-red solution (yellow for **7**) was cooled down to room temperature naturally and then filtrated to remove resulting precipitates. The crude product was obtained after the volatilization of solvent.

**Method B.** A mixture of  $(\text{Bu}_4\text{N})_4[\alpha\text{-Mo}_8\text{O}_{26}]$  (2.15 g, 1.0 mmol), DCC (0.43 g, 2.1 mmol), the hydrochloride salt of pyridine (0.15 g, 1.34 mmol) and amine (1.34 mmol, 0.17 g of 4-amino-*m*-cresol for **1**, 0.15 g of *p*-aminophenol for **3** and **4**, 0.21 g of 5-amino-1-naphenol for **6**) was refluxed at  $110$  °C in 20 mL of anhydrous acetonitrile. After about 12 h, the black-red solution was cooled down to room temperature naturally and then filtrated to remove resulting yellow precipitates. The black filtrate was allowed to crystallize in air, and the crude product was obtained after the volatilization of acetonitrile.

**Synthesis of Bifunctionalized Compounds.** A mixture of  $(\text{Bu}_4\text{N})_4[\alpha\text{-Mo}_8\text{O}_{26}]$  (2.15 g, 1.0 mmol), DCC (0.44 g, 2.2 mmol), and amine (0.25 g, 2.0 mmol, 0.25 g of 4-amino-*m*-cresol for **2**, 0.22 g of *p*-aminophenol for **5**) was refluxed at  $110$  °C in 15 mL of anhydrous acetonitrile under nitrogen. After 10–12 h, the black-red solution was cooled down to room temperature naturally and then filtrated to remove the resulting black precipitates. The black filtrate was allowed to vaporize in air. The black product was recrystallized twice from the mixture of acetone and EtOH(1:1).

**$(\text{Bu}_4\text{N})_2[\text{Mo}_6\text{O}_{18}(\text{Cres})]$  (**1**).** Compound **1** was obtained as black block crystals by recrystallization twice from the mixed solvent of acetone and EtOH(1:1). X-ray quality crystals were obtained in good yield of about 60 to 70% (based on Mo). <sup>1</sup>H NMR (300 MHz,  $\text{CD}_3\text{CN}$ , 300 K, TMS):  $\delta = 0.98(\text{t}, 24\text{H}, \text{CH}_3-, [\text{Bu}_4\text{N}]^+)$ ,  $1.60(\text{m}, 16\text{H}, -\text{CH}_2-)$ ,  $1.34(\text{m}, 16\text{H}, -\text{CH}_2-, [\text{Bu}_4\text{N}]^+)$ ,  $2.56(\text{s}, 3\text{H}, \text{CH}_3-, \text{CH}_3\text{Ar})$ ,  $3.4(\text{t}, 16\text{H}, \text{NCH}_2-, [\text{Bu}_4\text{N}]^+)$ ,  $7.06(\text{m}, 1\text{H}, \text{ArH})$ ,  $6.46(\text{m}, 1\text{H}, \text{ArH})$ ,  $6.7(\text{m}, 1\text{H}, \text{ArH})$ ,  $10.04(\text{s}, 1\text{H}, \text{Ar-OH})$ . IR (KBr,  $\text{cm}^{-1}$ ):  $3421(\text{broad}, \text{m})$ ,  $2962(\text{m})$ ,  $2933(\text{w}, \text{shoulder})$ ,  $2874(\text{m})$ ,  $1595(\text{m})$ ,  $1481(\text{m})$ ,  $1380(\text{w})$ ,  $1297(\text{w})$ ,  $975(\text{m}, \text{shoulder})$ ,  $953(\text{vs})$ ,  $877(\text{w})$ ,  $795(\text{vs})$ ,  $599(\text{w})$ . UV/vis (MeCN):  $\lambda_{\text{max}} = 365$  nm. Elemental Anal. for  $\text{C}_{39}\text{H}_{79}\text{Mo}_6\text{N}_3\text{O}_{19}$ : Calcd (%) C, 31.87; N, 2.86; H, 5.42. Found: C, 31.91; N, 2.90; H, 5.38.  $E_{1/2}$  (DMF):  $-0.762$  V.

**$(\text{Bu}_4\text{N})_2[\text{Mo}_6\text{O}_{17}(\text{Cres})_2] \cdot \text{H}_2\text{O}$  (**2**).** X-ray quality crystals were obtained in moderate yield of about 30 to 40% (based on Mo). <sup>1</sup>H NMR (300 MHz,  $\text{DMSO-d}_6$ , 300 K, TMS):  $\delta = 0.952(\text{t}, 12\text{H}, \text{CH}_3-, [\text{Bu}_4\text{N}]^+)$ ,  $1.562(\text{m}, 8\text{H}, -\text{CH}_2-)$ ,  $1.345(\text{m}, 8\text{H}, -\text{CH}_2-, [\text{Bu}_4\text{N}]^+)$ ,  $2.469(\text{s}, 3\text{H}, \text{CH}_3-, \text{CH}_3\text{-Ar})$ ,  $3.436(\text{t}, 8\text{H}, \text{NCH}_2-, [\text{Bu}_4\text{N}]^+)$ ,  $6.998(\text{m}, 1\text{H})$ ,  $6.589(\text{m}, 2\text{H}, \text{ArH})$ ,  $9.854(\text{s}, \text{Ar-OH})$ . IR (KBr,  $\text{cm}^{-1}$ ):  $3135(\text{m}, \text{br})$ ,  $2961(\text{m})$ ,  $2873(\text{m})$ ,  $1594(\text{s})$ ,  $1567(\text{m})$ ,  $1481(\text{s})$ ,  $1380(\text{w})$ ,  $1296(\text{s})$ ,  $1156(\text{w})$ ,  $969(\text{m}, \text{shoulder})$ ,  $948(\text{vs})$ ,  $877(\text{w})$ ,  $775(\text{vs})$ ,  $596(\text{w})$ . UV/vis (MeCN):  $\lambda_{\text{max}} = 365$  nm. Elemental Anal. for  $\text{C}_{46}\text{H}_{88}\text{Mo}_6\text{N}_4\text{O}_{20}$ : Calcd (%) C, 34.69; N, 3.52; H, 5.57. Found: C, 35.26; N, 3.50; H, 5.80.  $E_{1/2}$  (DMF):  $-1.011$  V.

**$(\text{Bu}_4\text{N})_2[\text{Mo}_6\text{O}_{18}(\text{Phen})] \cdot i\text{-PrOH}$  (**3**).** Compound **3** was obtained as black block crystals by recrystallization twice from the mixture of acetone and *i*-PrOH(1:1). X-ray quality crystals were obtained in good yield of about 65 to 75% (based on Mo). <sup>1</sup>H NMR (300 MHz,  $\text{DMSO-d}_6$ , 300 K, TMS):  $\delta = 0.959(\text{t}, 24\text{H}, \text{CH}_3-, [\text{Bu}_4\text{N}]^+)$ ,  $1.047(\text{d}, 6\text{H}, \text{CH}_3-i\text{-PrOH})$ ,  $1.573(\text{m}, 16\text{H}, -\text{CH}_2-)$ ,  $1.351(\text{m}, 16\text{H}, -\text{CH}_2-, [\text{Bu}_4\text{N}]^+)$ ,  $2.0854(\text{s}, 1\text{H}, -\text{CH}-i\text{-PrOH})$ ,  $3.195(\text{t}, 16\text{H}, \text{NCH}_2-, [\text{Bu}_4\text{N}]^+)$ ,  $4.344(\text{d}, 1\text{H}, \text{OH}-i\text{-PrOH})$ ,  $7.06(\text{m}, 1\text{H})$ ,  $6.7838(\text{d}, 2\text{H}, \text{ArH})$ ,  $7.110(\text{d}, 2\text{H}, \text{ArH})$ ,  $10.160(\text{s}, \text{Ar-OH})$ . IR (KBr,  $\text{cm}^{-1}$ ):  $3271(\text{m}, \text{br})$ ,  $2961(\text{s})$ ,  $2874(\text{s})$ ,  $1594(\text{s})$ ,  $1481(\text{s})$ ,  $1379(\text{m})$ ,  $1275(\text{s})$ ,  $1159(\text{m})$ ,  $975(\text{s}, \text{shoulder})$ ,  $953(\text{vs})$ ,  $880(\text{m})$ ,  $791(\text{vs})$ ,  $596(\text{m})$ . UV/vis (MeCN):  $\lambda_{\text{max}} = 359.5$  nm. Elemental Anal. for  $\text{C}_{41}\text{H}_{85}\text{Mo}_6\text{N}_3\text{O}_{20}$ : Calcd (%) C, 32.49; N, 2.77; H, 5.65. Found: C, 32.22; N, 2.69; H, 5.62.  $E_{1/2}$  (DMF):  $-0.753$  V.

**$(\text{Bu}_4\text{N})_2[\text{Mo}_6\text{O}_{18}(\text{Phen})] \cdot \text{EtOH}$  (**4**).** Compound **4** was recrystallized twice from a mixture of acetone and EtOH(1:1). X-ray quality crystals were obtained as black block crystals in good yield of about 60 to 70% (based on Mo). <sup>1</sup>H NMR (300 MHz,  $\text{DMSO-d}_6$ , 300 K, TMS):  $\delta = 0.965(\text{quintuple}, 24\text{H}, \text{CH}_3-, [\text{Bu}_4\text{N}]^+)$ ,  $1.108(\text{r}, 3\text{H}, \text{CH}_3-, \text{EtOH})$ ,  $1.575(\text{m}, 16\text{H}, -\text{CH}_2-)$ ,  $1.33(\text{m}, 16\text{H}, -\text{CH}_2-, [\text{Bu}_4\text{N}]^+)$ ,  $3.172(\text{s}, 16\text{H}, \text{NCH}_2-, [\text{Bu}_4\text{N}]^+)$ ,  $3.4371(\text{t}, 2\text{H}, -\text{CH}_2-, \text{EtOH})$ ,  $4.353(\text{s}, 1\text{H}, \text{OH}, \text{EtOH})$ ,  $7.110(\text{t}, 2\text{H}, \text{ArH})$ ,  $6.783(\text{t}, 2\text{H}, \text{ArH})$ ,  $10.185(\text{t}, 1\text{H}, \text{Ar-OH})$ . IR (KBr,  $\text{cm}^{-1}$ ):  $3271(\text{m}, \text{br})$ ,  $2962(\text{s})$ ,  $2933(\text{m}, \text{shoulder})$ ,  $2874(\text{m})$ ,  $1594(\text{s})$ ,  $1574(\text{m})$ ,  $1496(\text{m}, \text{shoulder})$ ,  $1482(\text{s})$ ,  $1471(\text{s})$ ,  $1379(\text{m})$ ,  $1275(\text{s})$ ,  $1218(\text{m})$ ,  $976(\text{m}, \text{shoulder})$ ,  $952(\text{vs})$ ,  $880(\text{w})$ ,  $791(\text{vs})$ ,  $596(\text{m})$ . UV/vis (MeCN):  $\lambda_{\text{max}} = 359.5$  nm. Elemental Anal. for  $\text{C}_{40}\text{H}_{83}\text{Mo}_6\text{N}_3\text{O}_{20}$ : Calcd (%) C, 31.99; N, 2.80; H, 5.57. Found: C, 31.55; N, 2.57; H, 5.59.  $E_{1/2}$  (DMF):  $-0.771$  V.

**$(\text{Bu}_4\text{N})_2[\text{Mo}_6\text{O}_{17}(\text{Phen})_2]$  (**5**).** X-ray quality crystals were obtained in low yield of about 20 to 30% (based on Mo). <sup>1</sup>H NMR (300 MHz,  $\text{DMSO-d}_6$ , 300 K, TMS):  $\delta = 0.956(\text{t}, 12\text{H}, \text{CH}_3-, [\text{Bu}_4\text{N}]^+)$ ,  $1.372(\text{sextuple}, 8\text{H}, -\text{CH}_2-)$ ,  $1.566(\text{m}, 8\text{H}, -\text{CH}_2-, [\text{Bu}_4\text{N}]^+)$ ,  $3.189(\text{t}, 8\text{H}, \text{NCH}_2-, [\text{Bu}_4\text{N}]^+)$ ,  $7.049(\text{d}, 2\text{H})$ ,  $6.7560(\text{d}, 2\text{H}, \text{ArH})$ ,  $9.993(\text{s}, 1\text{H}, \text{Ar-OH})$ . IR (KBr,  $\text{cm}^{-1}$ ):  $3036(\text{m}, \text{br})$ ,  $2961(\text{s})$ ,  $2931(\text{m}, \text{shoulder})$ ,  $2873(\text{s})$ ,  $1593(\text{s})$ ,  $1570(\text{m})$ ,  $1495(\text{m})$ ,  $1479(\text{s})$ ,  $1377(\text{m})$ ,  $1279(\text{s})$ ,  $1223(\text{m})$ ,  $1159(\text{m})$ ,  $970(\text{m}, \text{shoulder})$ ,  $955(\text{vs})$ ,  $840(\text{m}, \text{shoulder})$ ,  $778(\text{vs})$ ,  $585(\text{w})$ . UV/vis (MeCN):  $\lambda_{\text{max}} = 359.6$  nm. Elemental Anal. for  $\text{C}_{44}\text{H}_{82}\text{Mo}_6\text{N}_4\text{O}_{19}$ : Calcd (%) C, 34.17; N, 3.62; H, 5.34. Found: C, 34.53; N, 3.63; H, 5.40.  $E_{1/2}$  (DMF):  $-0.910$  V.

**$(\text{Bu}_4\text{N})_2[\text{Mo}_6\text{O}_{18}(\text{Naph})]$  (**6**).** X-ray quality crystals were obtained in good yield of about 60 to 70% (based on Mo). <sup>1</sup>H NMR (300 MHz,  $\text{DMSO-d}_6$ , 300 K, TMS):  $\delta = 0.949(\text{t}, 24\text{H}, \text{CH}_3-, [\text{Bu}_4\text{N}]^+)$ ,  $1.560(\text{m}, 16\text{H}, -\text{CH}_2-)$ ,  $1.340(\text{m}, 16\text{H}, -\text{CH}_2-, [\text{Bu}_4\text{N}]^+)$ ,  $2.56(\text{s}, 3\text{H}, \text{CH}_3-, \text{CH}_3\text{-Ar})$ ,  $3.183(\text{t}, 16\text{H}, \text{NCH}_2-, [\text{Bu}_4\text{N}]^+)$ ,  $8.082(\text{d}, 1\text{H}, \text{Ar-H})$ ,  $7.943(\text{d}, 1\text{H}, \text{Ar-H})$ ,  $7.500(\text{sextuple}, 2\text{H}, \text{Ar-H})$ ,  $7.383(\text{d}, 2\text{H}, \text{Ar-H})$ ,  $6.999(\text{d}, 1\text{H}, \text{Ar-H})$ ,  $10.429(\text{s}, 1\text{H}, \text{Ar-OH})$ . IR (KBr,  $\text{cm}^{-1}$ ):  $3267(\text{m}, \text{br})$ ,  $2961(\text{s})$ ,  $2931(\text{m}, \text{shoulder})$ ,  $2873(\text{m})$ ,  $1708(\text{w})$ ,  $1620(\text{w})$ ,  $1580(\text{m})$ ,  $1481(\text{s})$ ,  $1458(\text{s})$ ,  $1399(\text{m})$ ,  $1376(\text{m})$ ,  $1275(\text{m})$ ,  $1170(\text{w})$ ,  $1147(\text{w})$ ,  $1022(\text{m})$ ,  $975(\text{s}, \text{shoulder})$ ,  $954(\text{vs})$ ,  $879(\text{m})$ ,  $797(\text{vs})$ ,  $594(\text{m})$ . UV/vis (MeCN):  $\lambda_{\text{max}} = 406.5$  nm. Elemental Anal. for  $\text{C}_{42}\text{H}_{79}\text{Mo}_6\text{N}_3\text{O}_{19}$ : Calcd (%) C, 33.50; N, 2.79; H, 5.29. Found: C, 33.45; N, 2.80; H, 5.27.  $E_{1/2}$  (DMF):  $-0.752$  V.

Table 1. Crystallographic Data of Compounds 2–7

	2	3	4	5	6	7
formula	C <sub>46</sub> H <sub>88</sub> Mo <sub>6</sub> N <sub>4</sub> O <sub>20</sub>	C <sub>41</sub> H <sub>85</sub> Mo <sub>6</sub> N <sub>3</sub> O <sub>20</sub>	C <sub>40</sub> H <sub>83</sub> Mo <sub>6</sub> N <sub>3</sub> O <sub>20</sub>	C <sub>44</sub> H <sub>82</sub> Mo <sub>6</sub> N <sub>4</sub> O <sub>19</sub>	C <sub>42</sub> H <sub>79</sub> Mo <sub>6</sub> N <sub>3</sub> O <sub>19</sub>	C <sub>38</sub> H <sub>86</sub> Mo <sub>6</sub> N <sub>3</sub> O <sub>20.5</sub>
F. W.	1592.84	1515.76	1501.73	1546.78	1505.72	1488.74
crys. Sys.	triclinic	monoclinic	triclinic	orthorhombic	monoclinic	monoclinic
space group	<i>P</i> $\bar{1}$	<i>P</i> 2(1)/ <i>c</i>	<i>P</i> $\bar{1}$	<i>Pbcn</i>	<i>P</i> 2(1)/ <i>n</i>	<i>P</i> 2(1)/ <i>n</i>
<i>a</i> [Å]	12.846(3)	18.198(4)	12.604(3)	12.576(3)	19.288(4)	17.097(3)
<i>b</i> [Å]	12.969(3)	15.675(3)	13.104(3)	38.573(8)	14.917(3)	17.558(4)
<i>c</i> [Å]	21.060(4)	22.144(4)	19.371(4)	12.578(3)	20.143(4)	19.923(4)
$\alpha$ [deg]	85.65(3)	90	73.63(3)	90	90	90
$\beta$ [deg]	75.21(3)	113.61(3)	72.36(3)	90	106.37(3)	103.24(3)
$\gamma$ [deg]	72.69(3)	90	79.75(3)	90	90	90
<i>V</i> [Å <sup>3</sup> ]	3238.5(11)	5788(2)	2910.3(10)	6102(2)	5560.8(19)	5822(2)
<i>Z</i>	2	4	2	4	4	4
<i>D</i> <sub>calcd</sub> [g/cm <sup>3</sup> ]	1.633	1.74	1.714	1.684	1.799	1.698
$\mu$ [mm <sup>-1</sup> ]	1.193	1.329	1.321	1.262	1.382	1.32
<i>F</i> (000)	1608	3056	1512	3112	3024	3004
$\theta$ range [deg]	3.00 to 26.00	3.03 to 26.00	3.10 to 26.00	1.70 to 26.00	3.02 to 26.00	3.07 to 26.00
refl. collec.	21567	46993	25111	24903	46531	44864
<i>R</i> <sub>int</sub>	0.0443	0.0291	0.0351	0.0945	0.0257	0.0441
indep. refl.	11768	11366	11380	5762	10888	11157
GOF on <i>F</i> <sup>2</sup>	1.033	1.102	1.101	1.004	1.034	1.068
final <i>R</i> <sup><i>a</i></sup>	0.0563	0.0349	0.0427	0.0513	0.0283	0.0667
final <i>Rw</i> <sup><i>a</i></sup>	0.1687	0.0917	0.1276	0.1109	0.0776	0.1716

<sup>*a*</sup>  $R = \sum ||F_o| - |F_c|| / \sum |F_o|$  and  $Rw = [\sum [w(F_o^2 - F_c^2)^2] / \sum w(F_o^2)^2]^{1/2}$  with  $w = 1/[\sigma^2(F_o^2) + (aP)^2 + bP]$ , where  $P = (F_o^2 + 2F_c^2)/3$ . **2**:  $a = 0.0978$ ,  $b = 2.4572$ ; **3**:  $a = 0.0375$ ,  $b = 8.0298$ ; **4**:  $a = 0.0620$ ,  $b = 1.6474$ ; **5**:  $a = 0.0260$ ,  $b = 0$ ; **6**:  $a = 0.03995$ ,  $b = 3.6302$ ; **7**:  $a = 0.0024$ ,  $b = 92.4516$ .

(Bu<sub>4</sub>N)<sub>2</sub>[Mo<sub>6</sub>O<sub>18</sub>(Chex)]·1.5H<sub>2</sub>O (**7**). The yellow product was obtained through recrystallization twice from the mixture of acetone and toluene (1:1) usually in excellent yield of about 70 to 80% (based on Mo). <sup>1</sup>H NMR (300 MHz, Acetone-*d*<sub>6</sub>, 300 K, TMS):  $\delta = 0.98$ (t, 24H, CH<sub>3</sub>-, [Bu<sub>4</sub>N]<sup>+</sup>), 1.60(m, 16H, -CH<sub>2</sub>-), 1.34(m, 16H, -CH<sub>2</sub>-, [Bu<sub>4</sub>N]<sup>+</sup>), 2.56(s, 3H, CH<sub>3</sub>-, CH<sub>3</sub>-Ar), 3.4(t, 16H, NCH<sub>2</sub>-, [Bu<sub>4</sub>N]<sup>+</sup>), 7.06(m, 1H), 6.46(m, 1H, ArH), 6.7(m, 1H, ArH), 10.04(t, Ar-OH). IR (KBr, cm<sup>-1</sup>): 3533(m), 2961(s), 2935(m, shoulder), 2874(s), 1713(w), 1612(w), 1482(s), 1380(m), 1240(m), 1152(w), 1093(w), 1030(w), 977(m, shoulder), 954(vs), 795(vs), 662(m), 595(w). UV/vis (MeCN):  $\lambda_{\max} = 326$  nm. Elemental Anal. for C<sub>38</sub>H<sub>86</sub>Mo<sub>6</sub>N<sub>3</sub>O<sub>20.5</sub>: Calcd (%) C, 30.66; N, 2.82; H, 5.82. Found: C, 30.76; N, 2.65; H, 5.80. *E*<sub>1/2</sub> (DMF): -0.754 V.

## Discussion

**Synthesis.** In light of Errington's work, Peng et al. had developed a DCC-assisted dehydration protocol to yield organoimido derivatives of POMs.<sup>19a</sup> Subsequently, we have put forward an improved proton-promoted DCC protocol to prepare monofunctionalized derivatives in high yields and good purity by using hydrochloride salt of amine to replace free amine as imido-releasing source.<sup>25</sup> However, some hydrochloride salts of organic amine are difficult to be prepared and dried sometimes. We found that the mixture of hydrochloride salt of pyridine and amine could also play the same role as the hydrochloride salt of amine in the preparation of monofunctionalized imido derivatives of hexamolybdate. Herein, monofunctionalized products of compounds **1**, **3**, **4**, and **6** could be obtained by the protocol of hydrochloride salt of pyridine, as well as that of hydrochloride salt of amine. As far as we know, the yield of common bifunctionalized derivatives could be increased if the reaction time is prolonged from 12 h to 24 h.<sup>26</sup> However, it is not the same case in the preparation of bifunctionalized derivatives containing a remote hydroxyl group. In our early attempts to prepare compounds **2** and **5** using the conditions of refluxing for 24 h, none of the desired products were obtained. The

Brønsted acidity of hydroxyl is enhanced after being attached onto POMs through a multiply covalent bond, which perhaps results in some unwanted side reaction. We shortened the reaction time to 10–12 h, and then obtained the desired compounds **2** and **5** satisfactorily.

**Structure.** A summary of X-ray crystal data of compounds **2–7** is presented in Table 1. Oak Ridge thermal-ellipsoid plot (ORTEP) diagrams of the cluster anion of these seven compounds are shown in Figure 1 (Compound **1** had been mentioned simply in our previous communication,<sup>39</sup> which has been presented herein for better comparison and studied in detail). The selected bond lengths and angles are listed in Table 2, and the hydrogen bond data of compounds **1–7** are summarized in Table 4.

Compound **1** crystallizes in monoclinic system, *C*2/*c* space group; there is one crystallographically independent anion of [Mo<sub>6</sub>O<sub>18</sub>(NCres)]<sup>2-</sup> (Ar = *o*-CH<sub>3</sub>C<sub>6</sub>H<sub>3</sub>-*p*-OH) and two cations of (Bu<sub>4</sub>N)<sup>+</sup> in the asymmetric unit. As shown in Figure 1, the six molybdenum atoms in the anion cluster of [Mo<sub>6</sub>O<sub>18</sub>(NCres)]<sup>2-</sup> are bonded to the central oxygen atom O(1) to form a slightly distorted octahedral metal cage, with Mo···Mo separation ranging from 3.231(1) to 3.295(1) Å. All molybdenum atoms except Mo(1) are six-coordinated with one terminal oxygen atom (O<sub>t</sub>), four bridged oxygen atoms (O<sub>b</sub>), and one centered  $\mu_6$ -O(1) (O<sub>c</sub>) to form a distorted octahedron. For Mo(1), one terminal oxygen atom was substituted by the nitrogen atom from 4-hydroxy-2-methylaniline. As observed in other imido-hexamolybdates complexes (Table 3), the Mo–N bond in this compound also demonstrates substantial triple bond character, evidenced by the short bond length (1.726(3) Å) and nearly linear Mo–N–C angle (173.13°). Thus, an organic–inorganic hybrid conjugated system is constructed between the organic segments and the hexamolybdates cluster through the Mo≡N triple bond. As one consequence of the electronegativity of nitrogen atom being less than

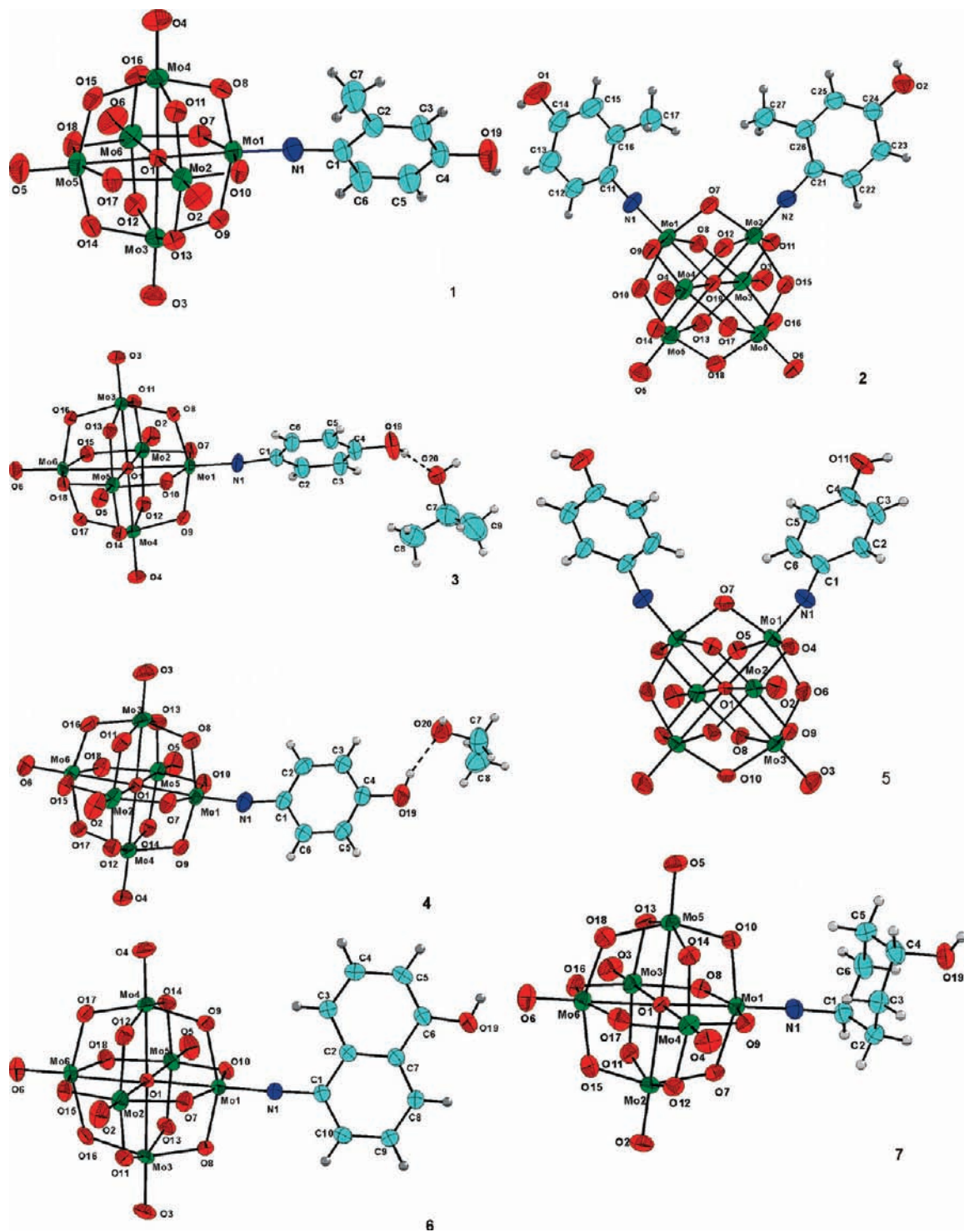


Figure 1. ORTEP drawing of anion clusters of compounds 1–7.

Table 2. Selected Bond Lengths and Bond Angles of Compounds 1–7

	1	2	3	4	5	6	7
C–N (Å)	1.395(5)	1.381(8), 1.386(8)	1.396(5)	1.397(5)	1.391(10)	1.398(4)	1.445(12)
Mo≡N (Å)	1.726(3)	1.739(6), 1.741(5)	1.726(3)	1.732(3)	1.715(7)	1.736(2)	1.728(8)
Mo–O <sub>i</sub> (Å)	1.677(3)–1.685(3)	1.688(4)–1.702(5)	1.673(3)–1.693(3)	1.678(3)–1.693(3)	1.687(4)–1.691(5)	1.681(2)–1.683(2)	1.662(8)–1.701(7)
Mo–O <sub>b</sub> (Å)	1.882(2)–1.988(2)	1.879(5)–2.013(5)	1.893(3)–1.956(3)	1.869(3)–1.981(4)	1.836(5)–2.018(4)	1.905(2)–1.952(2)	1.863(7)–1.981(6)
Mo–O <sub>c</sub> (Å)	2.210(2)–2.364(2)	2.232(4)–2.380(4)	2.234(2)–2.351(2)	2.213(2)–2.363(2)	2.220(5)–2.382(5)	2.2331(17)–2.3654(17)	2.234(6)–2.350(6)
Mo≡N–C (deg)	173.3(3)	171.7(6), 171.4(6)	172.4(3)	168.8(4)	162.3(6)	170.0(2)	177.0(8)

**Table 3.** Bond Length of C–N and Mo≡N and Bond Angle of Mo≡N–C in Some Reported Arylimido Derivatives

	Mo≡N(Å)	C–N(Å)	Mo≡N–C (deg)	ref.
[TBA] <sub>2</sub> [Mo <sub>6</sub> O <sub>18</sub> (NAr)]				
2,6-dimethylbenzenamine	1.724	1.402	178.33	19
4-ethynyl-2,6-dimethylbenzenamine	1.727	1.381	174.49	19
	1.729	1.357	172.61	
4-iodo-2,6-dimethylbenzenamine	1.733	1.398	165.92	19
	1.738	1.398	172.81	
4-fluoro-2-methylbenzenamine	1.727	1.384	174.68	16b
	1.734	1.399	174.46	
4-fluoro-benzenamine	1.724	1.388	174.09	16b
4-aminobenzonitrile	1.721	1.398	164.02	15b
o-toluidine	1.772	1.348	173.92	25
2,6-dimethyl-4-(2-(2,6-di(pyridin-2-yl)-pyridin-4-yl)ethynyl)benzenamine	1.747	1.375	175.80	18
4-chlorobenzenamine	1.686	1.433	163.62	25
4-bromobenzenamine	1.698	1.401	163.62	44c
[TBA] <sub>2</sub> [Mo <sub>6</sub> O <sub>17</sub> (NAr) <sub>2</sub> ]				
2-methoxybenzenamine	1.734, 1.738	1.384, 1.379	178.10 165.77	16a
2,6-diisopropyl-4-(2-(2,6-di(pyridin-2-yl)-pyridin-4-yl)ethynyl)benzenamine	1.738, 1.742	1.396, 1.386	176.58 170.53	18
	1.740	1.393	167.17	
	1.717	1.406	178.35	
2,6-dimethylbenzenamine	1.732, 1.724	1.382, 1.404	167.62 172.24	44a
o-toluidine	1.739, 1.722	1.384, 1.393	171.99 166.33	44b
4-ethynyl-2,6-dimethylbenzenamine	1.742, 1.750	1.378, 1.375	173.63 175.02	17b
4-iodo-2,6-dimethylbenzenamine	1.747, 1.749	1.380, 1.390	171.17 174.37	26
	1.745	1.382	172.24	
	1.744	1.378	172.84	
2,6-dimethylbenzenamine	1.739, 1.736	1.384, 1.397	178.39 172.46	26

that of oxygen atom, the bond length of Mo(1)≡N(1) (1.726(3) Å) is longer than that of Mo≡O<sub>t</sub> (1.677(3)–1.685(3) Å), and the Mo(1)–O(1) (2.210(2) Å) bond length of imido-bearing molybdenum atom is obviously shorter than that of other Mo–O(1) bonds (2.315(2)–2.364(2) Å) owing to the so-called “*trans influence*”; on the other hand, the average separation of Mo(1)···Mo (3.239 Å) is slightly shorter than that of other Mo···Mo (3.291 Å). As in other POMs clusters, alternating short and long bond length distortion (ABL) for Mo–O<sub>b</sub> resulting from a pseudo Jahn–Teller (PJT) vibronic instability was also observed in this anion cluster.<sup>27</sup>

Besides its interesting anion cluster structure, another interesting feature of compound **1** is the intermolecular hydrogen bonding interaction among neighboring cluster anions in the solid state. It was seen easily from Figure 2 that one cluster anion and two flanked neighbors along the *b* axis are first connected into 1D zigzag chain via O–H···O hydrogen bonds (O(19)–H(19)···O(7)<sup>#1</sup> 2.776(4) Å). Those chains are further connected into a 2D network with grid dimensions of 6 × 11 Å through interchain C–H···O hydrogen bonds (C(7)–H(7A)···O(11)<sup>#2</sup> 3.547(5) Å, C(7)–H(7A)···O(8)<sup>#2</sup> 3.645(2) Å, C(3)–H(3A)···O(4)<sup>#2</sup> 3.638(1) Å). One eight-membered ring with graph set symbol<sup>28</sup> of R<sub>2</sub><sup>2</sup> (8) is formed via C(7)–H(7A)···O(11)<sup>#2</sup> and C(3)–H(3A)···O(4)<sup>#2</sup>,

and one four-membered ring with graph set symbol of R<sub>2</sub><sup>1</sup> (4) is constructed by C(7)–H(7A)···O(11)<sup>#2</sup> and C(3)–H(3A)···O(4)<sup>#2</sup> among those adjacent chains.

Compound **2** crystallizes in triclinic crystal system, *P*1̄ space group. There are two cations of [Bu<sub>4</sub>N]<sup>+</sup>, one anion of [Mo<sub>6</sub>O<sub>17</sub>(NCres)<sub>2</sub>]<sup>2-</sup>, and one crystal water in the asymmetric unit. An ORTEP drawing of the anion is seen in Figure 1; two *cis* terminal oxo ligands of the hexamolybdate cluster were substituted by two imido ligands of 4-hydroxy-2-methylaniline. The short bond length of Mo–N (1.741(5) and 1.739(6) Å) and the linear angle Mo–N–C (176.8(2) and 177.8(2)°) are consistent with the multiple bond nature of Mo≡N and the sp hybrid mode of the N atom from the imido ligand. As one consequence of that the electron-donating ability of the imido ligand is superior to that of the oxo ligand, the bond lengths of Mo<sub>imido-bearing</sub>–O<sub>centreal</sub> (2.233(4) and 2.232(4) Å) are obviously shorter than those of other Mo–O<sub>centreal</sub> (2.359(4), 2.358(4), 2.380(4), and 2.376(4) Å) owing to the so-called “*trans influence*”, suggesting that the central oxo atom shifted slightly toward the imido-bearing molybdenum atoms. The long Mo–O<sub>b</sub> and short Mo–O<sub>b</sub> bonds also come forth alternately in the equatorial (Mo<sub>b</sub>)<sub>4</sub>(O<sub>b</sub>)<sub>4</sub> belt as observed as well in other POM clusters and **1**.

As seen in Figure 3, two hydrogen bonds of O(2)–H(2A)···O(8)<sup>#1</sup> and C(25)–H(25A)···O(11)<sup>#1</sup> form one eight-membered ring with the graph set symbol of R<sub>2</sub><sup>2</sup> (8). The adjacent two [Mo<sub>6</sub>O<sub>17</sub>(NCres)<sub>2</sub>]<sup>2-</sup> are connected into a dimer through two pairs of hydrogen bond rings.

(28) Bernstein, J.; Davis, R. E.; Shimoni, L.; Chang, N.-L. *Angew. Chem., Int. Ed.* **1995**, *33*, 143.

**Table 4.** Summary of Hydrogen Bonding in Compounds 1–7

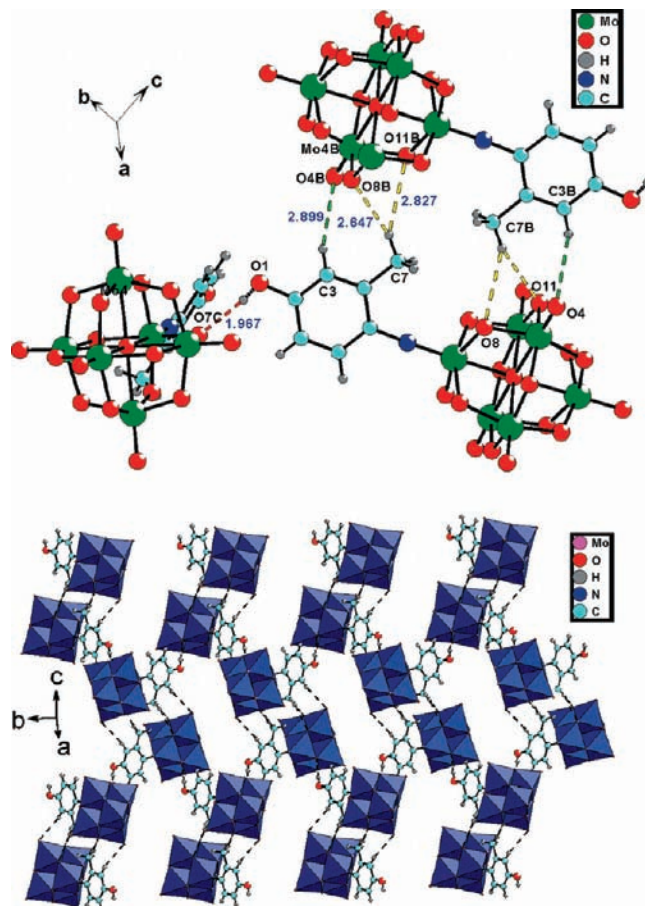
D–H···A	<i>d</i> (H···A)	<i>d</i> (H···A)	<i>d</i> (D···A)	<(DHA)
Compound 1 <sup>a</sup>				
O(19)–H(19)···O(7) <sup>#1</sup>	0.82	1.97	2.776(4)	168.7
C(7)–H(7A)···O(11) <sup>#2</sup>	0.96	2.65	3.547(5)	156.0
C(7)–H(7A)···O(8) <sup>#2</sup>	0.96	2.83	3.645(2)	143.68
C(3)–H(3A)···O(4) <sup>#2</sup>	0.93	2.90	3.638(1)	137.4
Compound 2 <sup>b</sup>				
O(1)–H(1 <sup>a</sup> )···O(20)	0.82	1.96	2.776(13)	175.8
O(2)–H(2 <sup>a</sup> )···O(8) <sup>#1</sup>	0.82	1.84	2.648(7)	169.8
O(20)–H(20B)···O(15) <sup>#2</sup>	0.78(5)	2.03(7)	2.778(10)	161(15)
C(25)–H(25A)···O(11) <sup>#1</sup>	0.93	2.53	3.386(9)	153
Compound 3 <sup>c</sup>				
O(19)–H(19A)···O(20)	0.82	1.90	2.705(7)	168.4
O(20)–H(20A)···O(18) <sup>#1</sup>	0.82	2.18	2.868(5)	142.0
Compound 4 <sup>d</sup>				
O(19)–H(19A)···O(20)	0.82	1.94	2.735(6)	163.5
C(3)–H(3A)···O(13) <sup>#1</sup>	0.93	2.57	3.451(6)	159.4
C(8)–H(8B)···O(16) <sup>#1</sup>	0.96	2.69	3.402(69)	131.2
Compound 5 <sup>e</sup>				
O(11)–H(11)···O(4) <sup>#4</sup>	0.82	1.86	2.610(6)	152.0
C(5)–H(5)···O(11) <sup>#2</sup>	0.93	2.60	3.434(11)	150.3
Compound 6 <sup>f</sup>				
O(19)–H(19A)···O(14) <sup>#1</sup>	0.82	2.04	2.849(3)	167.5
C(5)–H(5A)···O(10) <sup>#1</sup>	0.93	2.53	3.447(30)	166.3
C(3)–H(3A)···O(9)	0.93	2.74	3.644(18)	163.7
C(9)–H(9A)···O(3) <sup>#2</sup>	0.93	2.52	3.267(35)	137.8
Compound 7 <sup>g</sup>				
C(1)–H(1A)···O(7) <sup>#1</sup>	0.98	2.52	3.371(11)	144.4
O(1W)–H(1WC)···O(7)	0.82	2.30	3.006(11)	144.3
O(1W)–H(1WA)···O(8) <sup>#1</sup>	0.85	2.26	3.094(11)	168.1
O(19)–H(19A)···O(16) <sup>#2</sup>	0.82	2.26	2.994(11)	149.7

<sup>a</sup> Symmetry code: <sup>#1</sup>  $-x + 1/2, y + 1/2, -z + 1/2$  <sup>#2</sup>  $-x + 1/2, -y - 1/2, -z + 1$ . <sup>b</sup> Symmetry code: <sup>#1</sup>  $-x + 1, -y + 1, -z + 2$  <sup>#2</sup>  $x + 1, y - 1, z$ . <sup>c</sup> Symmetry code: <sup>#1</sup>  $x, y - 1, z$ . <sup>d</sup> Symmetry code: <sup>#1</sup>  $-x, -y + 1, -z + 2$ . <sup>e</sup> Symmetry code: <sup>#2</sup>  $-x, y, -z + 1/2$ ; <sup>#4</sup>  $-x + 1/2, -y + 1/2, z - 1/2$ . <sup>f</sup> Symmetry code: <sup>#1</sup>  $-x + 1, -y, -z + 1$  <sup>#2</sup>  $-x + 3/2, y - 1/2, -z + 1/2$ . <sup>g</sup> Symmetry code: <sup>#1</sup>  $-x + 2, -y + 1, -z$  <sup>#2</sup>  $x - 1/2, -y + 1/2, z - 1/2$ .

Those dimers are further linked into a 1D wavelike infinite double chain along the *a* axis using the water of crystallization as a bridge through the two hydrogen bonds of O(1)–H(1A)···O(20) and O(20)–H(20B)···O(15)<sup>#2</sup>.

Compound 3, a monofunctionalized derivative of *p*-aminophenol (Phen), crystallizes in the monoclinic system  $P2_1/c$  space group. There are two cations of [Bu<sub>4</sub>N]<sup>+</sup>, one anion of [Mo<sub>6</sub>O<sub>18</sub>(NPhen)]<sup>2-</sup>, and one molecule of *i*-PrOH in the asymmetric unit. The anion cluster structure (Figure 1) is similar to that of compound 1 except that the ligand of Cres is replaced by Phen. Compound 4 crystallizes in triclinic system,  $P\bar{1}$  space group. The anion cluster of 4 is the same as that of 3 except that the solvent molecule of *i*-PrOH is replaced by EtOH.

Different solvent molecules in 3 and 4 resulted in their different hydrogen bonding interactions. Those anion clusters in compound 3 are connected into a 1D infinite wavelike chain using the solvent molecule of *i*-PrOH as bridge through the O(19)–H(19A)···O(20) and O(20)–H(20A)···O(18)<sup>#1</sup> hydrogen bonds (Figure 4,

**Figure 2.** Basic hydrogen bonding building block of compound 1 (top) and the polyhedral viewing of the 2D hydrogen bonding network of compound 1 (bottom).

Supporting Information, Figure S1). While in compound 4 the neighboring two cluster anions are connected into one dimer through two C–H···O hydrogen bonds C(3)–H(3A)···O(13)<sup>#1</sup>, and the outward two hydroxyls from the two anions are occluded by two flanked EtOH molecules to form a dimer through the hydrogen bonds of O(19)–H(19A)···O(20) and O(20)–H(20A)···O(18)<sup>#1</sup>. The C–H···O interaction of C(8)–H(8B)···O(16)<sup>#1</sup> combines with other two hydrogen bonds of O(19)–H(19A)···O(20) and O(20)–H(20A)···O(18)<sup>#1</sup> to form one 12-membered hydrogen bonding ring ( $R_3^3(12)$ ) (Figure 5).

Compound 5, a *cis* bifunctionalized derivative of 4-hydroxyaniline, crystallizes in orthorhombic system,  $Pbcn$  space group. There are one-half of the anion of [Mo<sub>6</sub>O<sub>17</sub>(NC<sub>6</sub>H<sub>4</sub>OH)<sub>2</sub>]<sup>2-</sup> and two half cations of [Bu<sub>4</sub>N]<sup>+</sup> in the asymmetric unit. As shown in Figure 1. Two terminal oxo ligands of hexamolybdate in the *cis* position are substituted by two imido ligands of ≡NC<sub>6</sub>H<sub>4</sub>OH, and the whole anion cluster has a symmetry plane across the O1, O7, and O5 atoms. The neighboring cluster anions are first connected with one another into one 1D wavelike infinite chain through one pair of C–H···O hydrogen bonds of C(5)–H(5)···O(11)<sup>#2</sup>, which forms one eight-membered hydrogen bonding ring ( $R_2^8(8)$ ). And those chains are further connected into 2D hydrogen networks by interchain O–H···O hydrogen bonds of O(11)–H(11)···O(4)<sup>#4</sup> (Figure 6).



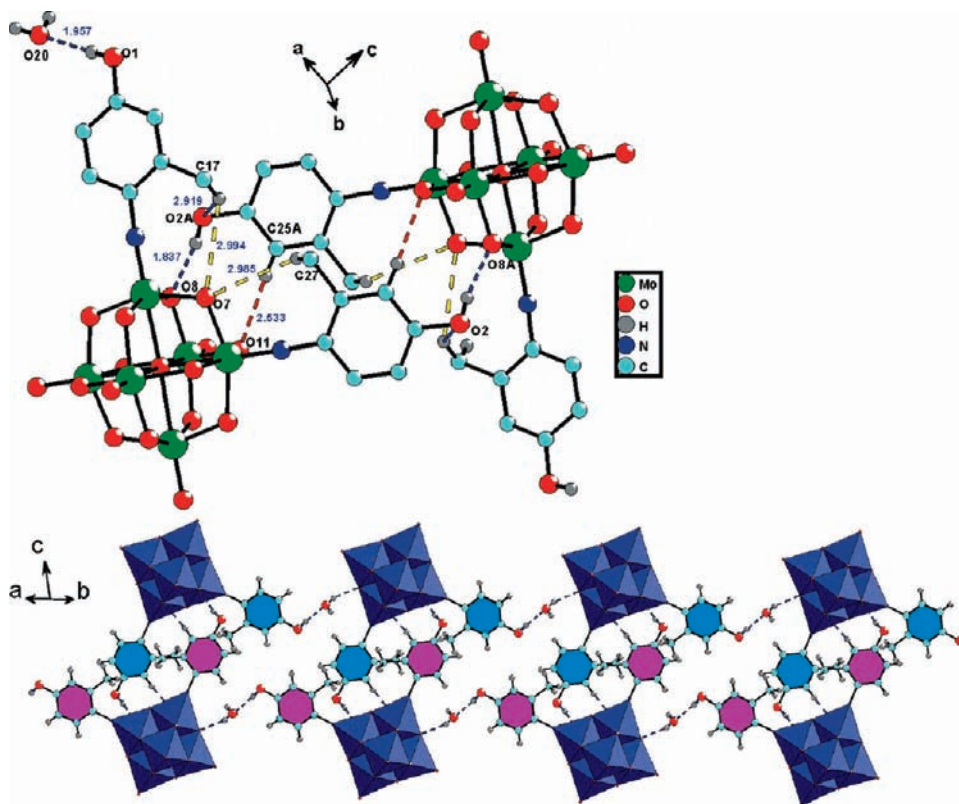


**Figure 3.** Basic hydrogen bonding building block of compound 2 (top) and the polyhedral viewing of the 1D infinite double chain of compound 2 (bottom).

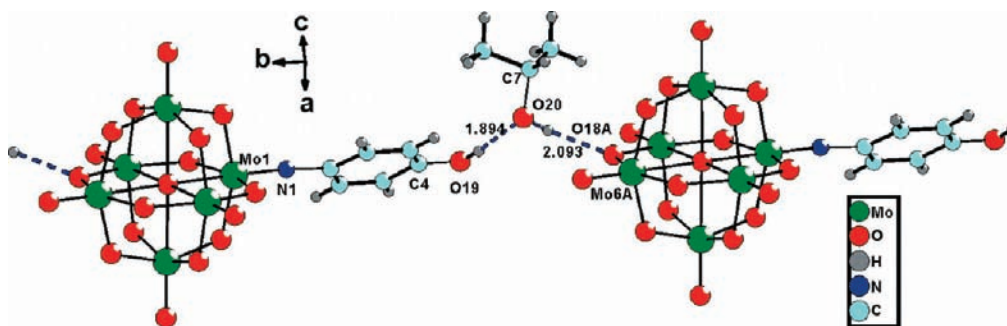


**Figure 4.** Basic hydrogen bonding building block of compound 3.

Compound 6, a monofunctionalized derivative of Naph, crystallizes in monoclinic system,  $P2_1/n$  space group. There are one anion of  $[\text{Mo}_6\text{O}_{18}(\text{Naph})]^{2-}$  and two cations of  $[\text{Bu}_4\text{N}]^+$  in the asymmetric unit. The cluster anion (Figure 1) is similar to that of other monofunctionalized derivatives except that the ligand was replaced by Naph. One intramolecular C–H $\cdots$ O hydrogen bonding of C(3)–H(3A) $\cdots$ O(9) forms one seven-membered ring ( $R_1^1$  (7)) (Figure 7). The neighboring two cluster anions form one dimer through one pair of intermolecular hydrogen bonding ring ( $R_2^2$  (8)) which are formed by O(19)–H(19A) $\cdots$ O(14) $^{\#1}$  and C(5)–H(5A) $\cdots$ O(10) $^{\#1}$ . The distance of the center of ring from two Naph is 4.308 Å, and the plane distance between adjacent naph rings in the dimer is 3.290 Å, indicating the presence of strong  $\pi$ – $\pi$  interaction between the adjacent two Naph rings. The dimer provides two outward C–H bonds as hydrogen bond donor and two bridged oxo

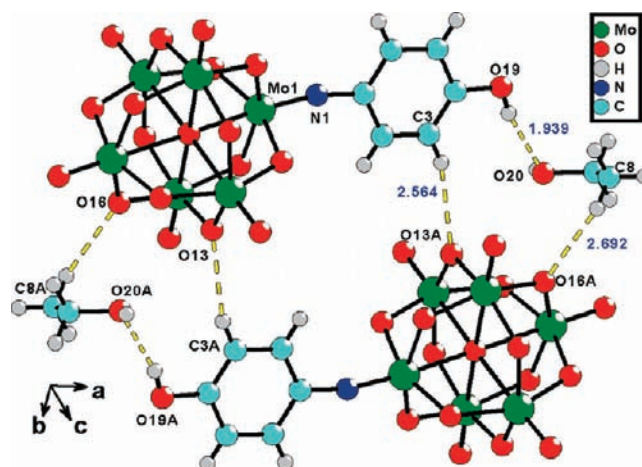


**Figure 5.** Hydrogen bonding dimer of compound 4.

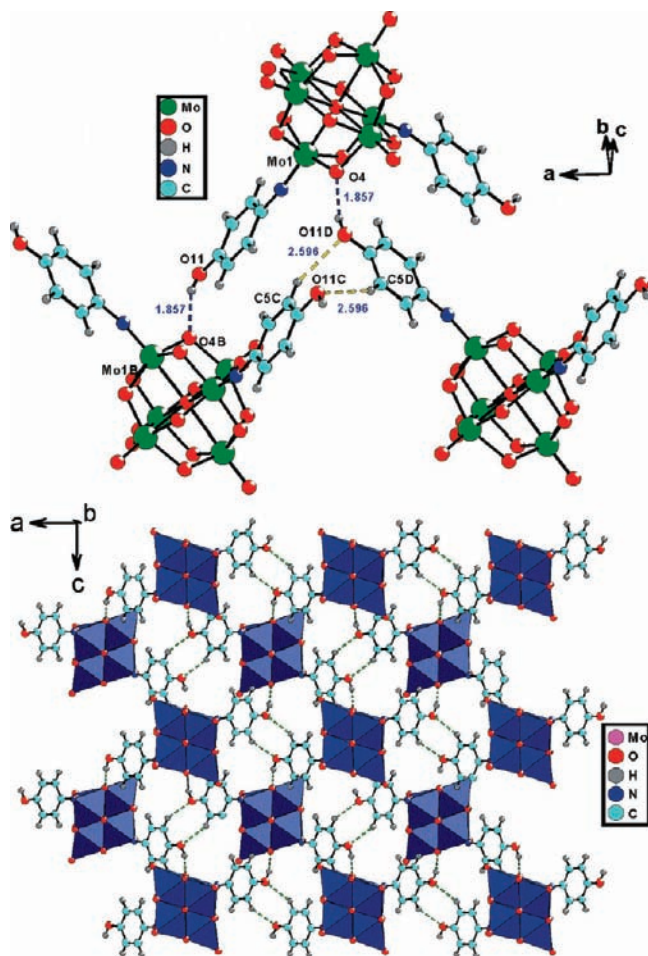


**Figure 6.** Basic hydrogen bonding building block of compound **5** (top) and the polyhedral view of the 2D hydrogen bonding network of compound **5** (bottom).

ligands as hydrogen bond acceptor to form a 4-connected 2D hydrogen bonding network with  $7 \times 20$  Å “Z” type grid (Figure 7, Supporting Information, Figure S2).

Compound **7**, a monofunctionalized derivative of Chex, crystallizes in monoclinic system  $P2_1/n$  space group. There are one anion of  $[\text{Mo}_6\text{O}_{18}\text{N}(\text{Chex})]^{2-}$ , two cations of  $[\text{Bu}_4\text{N}]^+$ , and one and a half molecules of crystalline water in the asymmetric units. An ORTEP drawing of the anion is shown in Figure 1. The cluster anion is generally similar to that of other monofunctionalized derivatives except that the organic ligand is replaced by one imido ligand of Chex. The neighboring two anionic clusters first form one dimer through two nine-membered hydrogen bonding rings ( $R_3^3$  (9)) which are formed by one C–H $\cdots$ O hydrogen bond (C(1)–H(1A) $\cdots$ O(7) $^{\#1}$ ) and two O–H $\cdots$ O hydrogen bonds (O(1W)–H(1WC) $\cdots$ O(7), O(1W)–H(1WA) $\cdots$ O(8) $^{\#1}$ ) (Figure 8). These dimers are further connected into one four-connected 2D network through two outward hydroxyls as hydrogen bonding donors and two bridged oxo atoms of O16 and O16B as hydrogen bonding acceptors. There are interlaced “8” type pores with dimension of  $17.5 \times 9.6$  Å ( $5.7$  Å for narrow) in the framework (Figure 8, Supporting Information, Figure S3).

Besides its influences on cell packing, hydrogen bonding also has a distinct influence on the conformation of

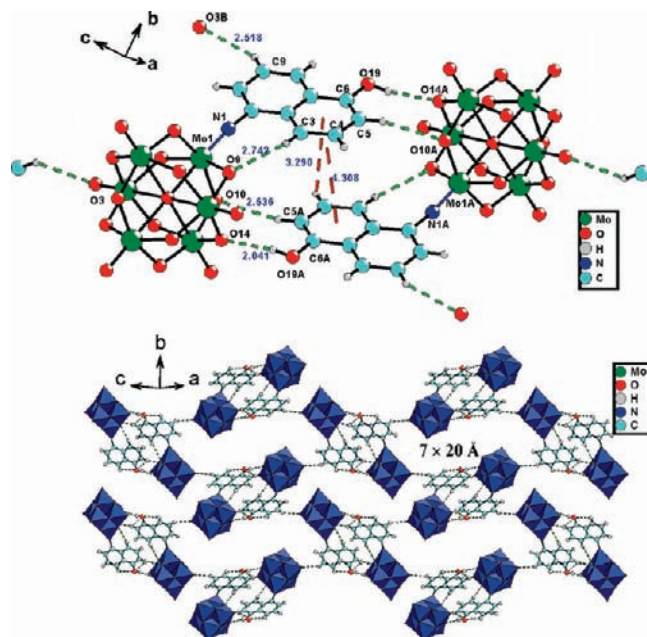


**Figure 7.** Basic hydrogen bonding building block of compound **6** (top) and the polyhedral view of the 2D hydrogen bonding network of compound **6** (bottom).

the cluster anions. The cluster anions of arylimido derivatives of hexamolybdate have various conformations if the rotatable C–N bond in those anion clusters stand at different positions. The conformation of the anion cluster could be defined by the dihedral angle between the aryl plane and the attached longitudinal  $\text{Mo}_4\text{O}_4$  plane for monofunctionalized derivatives; as for bifunctionalized derivatives, it is defined as the dihedral angle between the aryl plane and the attached common longitudinal  $\text{Mo}_4\text{O}_4$  plane (as shown in Supporting Information, Figure S4). The dihedral angles of these compounds **1–6** are summarized in Supporting Information, Table S1. It is easy to see that the dihedral angles in those compounds are all deviated from the ideal zero degrees more or less to accommodate their different intramolecular hydrogen bonding interactions. The most typical examples are the cluster anions of compounds **2** and **5** which are bifunctionalized organoimido derivatives of hexamolybdate; two bound aryl ring (the ring of C11 to C16 and the ring of C21 to C26) in compound **2** are nearly coplanar with a shared  $\text{Mo}_4\text{O}_4$  plane (Mo1, Mo2, Mo5, Mo6, O7, O10, O15 and O18) with the dihedral angles of  $13.4$  and  $14.5^\circ$ , while for compound **5** the dihedral angles between the  $\text{Mo}_4\text{O}_4$  ring and the two Phen rings are  $62.3$  and  $62.3^\circ$ , seriously deviated from the ideal coplanar conformation owing to the formation of intermolecular C–H $\cdots$ O hydrogen bonding (C(5)–H(5) $\cdots$ O(11) $^{\#2}$ ).

Several conclusions could be drawn upon the analysis of the hydrogen bonding mode in those compounds: first, bridged oxo ligands in these remote hydroxyl functionalized organoimido hexamolybdates are more inclined to form hydrogen bonding as acceptors than terminal oxo ligands because the bridged oxo ligands as acceptors in those compounds could result in a more compact cell packing, in accordance with the lowest energy principle; second, small solvent molecules with hydrogen bonding donors and acceptors play an important role in their

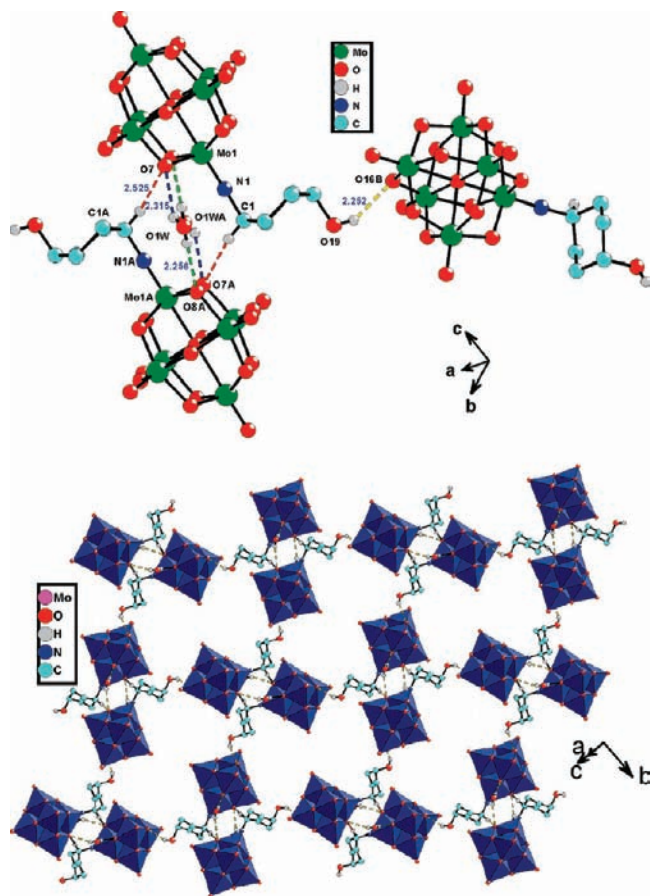


**Figure 8.** Basic hydrogen bonding building block of compound **7** (top) and the polyhedral view of the 2D hydrogen bonding network of compound **7** (bottom).

hydrogen bonding assembly, and different solvent molecules may result in their different cell packing; third, cooperative hydrogen bonds forming the hydrogen bonding ring are found in many cases; fourth, intermolecular and intramolecular hydrogen bonds not only influence their cell packing but also have an important impact on the cluster's conformation.

Owing to the differences of the electron-donating ability of substituted ligands and substituted extent, different organoimido ligands can produce a different influence on the electron density on the hexamolybdate cluster, which can be slightly reflected to some extent on the size change of the cluster skeleton: it is obvious that the skeleton size will be enlarged to disperse redundant electron density if it is attached with an electron-donating ligand, whereas it will shrink if it is attached by the electron-withdrawing ligand in theory.<sup>30</sup> We herein define the cluster skeleton size using three parameters: averaged neighboring Mo···Mo distance, averaged M–O<sub>b</sub> distance, and averaged Mo–O<sub>c</sub> distance. The cluster skeleton parameters of compounds **1–7** are summarized in Table 5. It is obvious that the cluster skeleton size parameter of compound **1**, **3**, **4**, and **6** are similar to that of their parent cluster, that is, because there are two kind of electronic interaction in those cluster. One is the arylimido as electron-donating ligand to give partly  $\pi$  electrons to the bound hexamo-

**Table 5.** Summary of the Cluster Skeleton Parameters of Compounds **1–7** and Hexamolybdates

compound	Mo···Mo (Å)	Mo–O <sub>b</sub> (Å)	Mo–O <sub>c</sub> (Å)
(TBA) <sub>2</sub> [Mo <sub>6</sub> O <sub>19</sub> ] <sup>a</sup>	3.274	1.922	2.315
<b>1</b>	3.274	1.923	2.315
<b>2</b>	3.285	1.929	2.323
<b>3</b>	3.276	1.921	2.316
<b>4</b>	3.274	1.923	2.315
<b>5</b>	3.273	1.931	2.315
<b>6</b>	3.275	1.924	2.316
<b>7</b>	3.283	1.927	2.321

<sup>a</sup> The cluster skeleton parameters of (TBA)<sub>2</sub>[Mo<sub>6</sub>O<sub>19</sub>] are obtained and averaged according to our unpublished results.

lybdate, and another one is that the vacant  $\pi$  orbital of aryl ligand could accommodate feedback negative charge from the hexamolybdate cluster; the two kinds of interaction are possibly equivalent in those compounds. However, in compound **2**, the electron-donating interaction of the ligands cluster is larger than the feedback interaction of the POMs owing to the increase of the substituted extent, and thereby the cluster skeleton size parameters are larger than those of corresponding monofunctionalized derivatives. Compound **7** demonstrates a larger cluster skeleton size parameter than other monofunctionalized derivatives owing to the lack of electron feedback interaction. Compound **5** unexpectedly demonstrates a similar cluster skeleton size compared to the corresponding monofunctionalized derivatives; one possible reason is the balanced results of the two kinds of interaction, and another reason is that this compound crystallizes in a space group with a higher symmetry, which results in a more compact cell packing of compound **5**.

Pyykkö et al. had predicted theoretically that the maximal bond length of a full Mo≡N bond is 1.67 Å,<sup>29</sup> but the observed bond length of arylimido hexamolybdate is usually beyond 1.70 Å (as shown in Tables 2 and 3), for example, in our case, the bond lengths of Mo≡N are 1.726(3) Å for **1**, 1.739(6), 1.741(5) Å for **2**, 1.726(3) Å for **3**, 1.732(3) Å for **4**, 1.715(7) Å for **5**, 1.736(2) Å for **6**, and 1.728(8) Å for **7**, respectively. This is because the negative charges of hexamolybdates decrease the intensity of Mo≡N bond length; on the other hand, conjugation of the hexamolybdates cluster with arylimido ligands also elongate the length of the Mo≡N bonds. To take no account of the electronic influence of remote functional groups and the crystal data quality, the bond lengths of Mo≡N (1.70–1.73 Å) for monofunctionalized derivatives are slightly shorter than that of bifunctionalized derivatives (1.73–1.74 Å) in the mass, it is because the hexamolybdates cluster in bifunctionalized derivatives bears more electronic density than that of monofunctionalized derivatives owing to the accumulation effect of electron density with the increase of substituent number, which reduces the electron withdrawing ability of the hexamolybdates cluster in bifunctionalized derivatives and result in their longer Mo≡N bond in comparison with that of monofunctionalized derivatives, especially for those monofunctionalized and bifunctionalized derivatives containing the same ligands. The bond lengths of C–N in arylimido derivatives are in the range of 1.348–1.433 Å, slightly shorter than that of C–N single bond, confirming the delocalized feature in those anions

(29) Pyykkö, P.; Riedel, S.; Patzschke, M. *Chem.—Eur. J.* **2005**, *11*, 3511.

(30) Bridgeman, A. J.; Cavigliasso, G. *Inorg. Chem.* **2002**, *41*, 1761.

**Table 6.** Summary of the Lowest Energy Absorption of UV Spectra of Compounds 1–7 and Corresponding Imido-Hexamolybdates without Hydroxyl Group

compound	$\lambda$ , nm	ref.	compound	$\lambda$ , nm
[TBA] <sub>2</sub> [Mo <sub>6</sub> O <sub>19</sub> ]	320	19a		
[TBA] <sub>2</sub> [Mo <sub>6</sub> O <sub>18</sub> (NC <sub>6</sub> H <sub>5</sub> -Me-o)]	350	25,41	<b>1</b>	365
[TBA] <sub>2</sub> [Mo <sub>6</sub> O <sub>12</sub> (NC <sub>6</sub> H <sub>5</sub> -Me-o) <sub>2</sub> ]	354	41,44b	<b>2</b>	365
[TBA] <sub>2</sub> [Mo <sub>6</sub> O <sub>18</sub> (NC <sub>6</sub> H <sub>5</sub> ) <sub>2</sub> ]	342	44d	<b>3, 4</b>	359.5
[TBA] <sub>2</sub> [Mo <sub>6</sub> O <sub>17</sub> (NC <sub>6</sub> H <sub>5</sub> ) <sub>2</sub> ]			<b>5</b>	359.6
[TBA] <sub>2</sub> [Mo <sub>6</sub> O <sub>18</sub> (NC <sub>10</sub> H <sub>9</sub> ) <sub>2</sub> ]	383	16c	<b>6</b>	406.4
[TBA] <sub>2</sub> [Mo <sub>6</sub> O <sub>18</sub> (NC <sub>6</sub> H <sub>11</sub> ) <sub>2</sub> ]	325	24,42b	<b>7</b>	326

resulting from the d- $\pi$  interaction between the organic segments and hexamolybdates cluster.

**UV/vis Absorption Spectra.** The electronic properties of the seven compounds were studied by UV/vis absorption spectra. The lowest energy L $\rightarrow$ M electronic transition in the [Mo<sub>6</sub>O<sub>19</sub>]<sup>2-</sup> parent is found around 325 nm, while for compound **1**, **2**, **3**, **4**, **5**, **6**, and **7**, the lowest energy electronic transition appeared around 365, 365, 359.5, 359.5, 359.6, 406.4, and 326 nm, respectively (Table 6). The large bathochromic shift of the lowest energy electronic transition in compounds **1–6** indicates the presence of a strong d- $\pi$  electronic interaction between the hexamolybdate cluster and the arylimido ligands. Especially, the lowest energy electronic transition of compound **6** is found to shift bathochromically to 406.5 nm owing to the extension of the conjugated system. As for compounds **7**, it shows only negligible bathochromic shift of the lowest energy electronic transition because of short of  $\pi$  orbital in the grafting alkylimido ligand. Owing to the introduction of a strong electron-donating hydroxyl group, a kind of good auxochrome, the lowest energy electronic transition of those remote hydroxyl functionalized conjugated arylimido derivatives (**1–6**) have a bathochromic shift about 15–23.5 nm in comparison with that of the corresponding arylimido derivatives without hydroxyl group.

**FT-IR Spectra.** FT-IR spectra of compounds **1**, **3**, **4**, **6**, and **7** demonstrate some similar features as well as that of other monofunctionalized imido derivatives. In the IR spectra of hexamolybdate, two strong peaks of Mo–O<sub>t</sub> and Mo–O<sub>b</sub>–Mo appear at 957 and 798 cm<sup>-1</sup>, respectively. In compounds **1**, **3**, **4**, **6**, and **7**, the peaks of Mo≡O<sub>t</sub> are found to split into two peaks with about 20 cm<sup>-1</sup> intervals. A shoulder peak around 975 cm<sup>-1</sup> (975 for **1**, 975 for **3**, 976 for **4**, 975 for **6**, and 977 for **7**) is tentatively ascribed as the Mo≡N stretching vibration,<sup>31</sup> and the strong peak around 953 cm<sup>-1</sup> (953 cm<sup>-1</sup> for **1**, 953 cm<sup>-1</sup> for **3**, 953 cm<sup>-1</sup> for **4**, 954 cm<sup>-1</sup> for **6**, 954 cm<sup>-1</sup> for **7**) is attributed to the Mo≡O<sub>t</sub> stretching vibration. The Mo–O<sub>b</sub>–Mo stretching vibration is found at 795 cm<sup>-1</sup> in **1**, 791 cm<sup>-1</sup> in **3**, 791 cm<sup>-1</sup> in **4**, 797 cm<sup>-1</sup> in **6**, and 797 cm<sup>-1</sup> in **7**, respectively, demonstrating a slight red-shift compared to that in [Mo<sub>6</sub>O<sub>19</sub>] owing to the modification by one organoimido ligand. As for bifunctionalized derivatives of compound **2** and **5**, the Mo≡N, Mo≡O<sub>t</sub>, and Mo–O<sub>b</sub>–Mo stretching vibration are found to appear at 969 cm<sup>-1</sup>, 948 cm<sup>-1</sup>, and 775 cm<sup>-1</sup> in **2**, at 970 cm<sup>-1</sup>, 955 cm<sup>-1</sup>, and 777 cm<sup>-1</sup> in **5**, respectively, in which the Mo–O<sub>b</sub>–Mo stretching vibration shows a large red shift

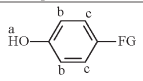
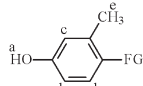
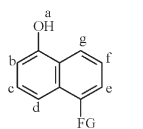
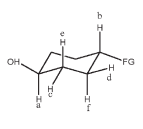
in comparison with that of [Mo<sub>6</sub>O<sub>19</sub>]<sup>2-</sup> and quite different from those monofunctionalized derivatives. It is obvious that the stretching vibration of Mo≡N, Mo≡O<sub>t</sub>, and Mo–O<sub>b</sub>–Mo have an increasing red shift with the increase of substituent extent. Owing to the formation of hydrogen bonding in those compounds, the OH stretching vibration is found as a broad medium peak around 3400 cm<sup>-1</sup> in **1**, 3100 cm<sup>-1</sup> in **2**, 3250 cm<sup>-1</sup> in **3**, 3250 cm<sup>-1</sup> in **4**, 3100 cm<sup>-1</sup> in **5**, 3270 cm<sup>-1</sup> in **6**, and 3500 cm<sup>-1</sup> in **7**, respectively.

**<sup>1</sup>H NMR Spectra.** The <sup>1</sup>H NMR spectra of compounds **2–6** in *d*<sub>6</sub>-DMSO (CD<sub>3</sub>CN for **1**) solution shows clearly resolved signals, all of which can be unambiguously assigned. The integration matches well with their structures. The <sup>1</sup>H NMR chemical shifts of aryl hydrogen atoms in compounds **1–7**, corresponding free amines, and nitro compounds are summarized in Table 7. Owing to the electron-withdrawing effect of attached POMs cluster, the aryl hydrogen atoms and the hydroxyl hydrogen atoms in monosubstituted derivatives, such as compounds **1**, **3**, **4**, and **6**, demonstrate obvious downfield shifts compared to that of corresponding free amines, but their downfield shifts are slightly smaller than that of corresponding nitro compounds. Because of the extension of the delocalized system, the –OH of compound **6** demonstrates larger downfield chemical shifts than those of compounds **1**, **3**, and **4**, showing that the –OH Brønsted acidity of compound **5** is stronger than that of compounds **1**, **3**, and **4**. Owing to the accumulation effect of electron density, the electron-drawing ability of functionalized hexamolybdates cluster shows a step-down trend with the increase of the number of substituents. Therefore, the aryl hydrogen atoms and hydroxyl hydrogen atoms of double substituted derivatives (compounds **2**, **5**) demonstrate a slight upfield shift compared with that of corresponding monosubstituted derivatives (**1**, **3**, **4**). The <sup>1</sup>H NMR spectrum of **7** was performed in *d*<sub>6</sub>-acetone solution for clearer signals. <sup>1</sup>H NMR resonance signal of the  $\beta$  hydrogen in Chex is found to stand downfield (4.44 ppm) compared to that of the hydroxyl group in Chex (3.77 ppm) owing to the electron-drawing influence of hexamolybdates, indicating the enhanced Brønsted acidity of the  $\beta$  hydrogen in the Chex ligand of compound **7**, which is even stronger than that of ROH, that possibly answers for the origin of the  $\beta$  C–H bond activation in alkylimido derivatives of POMs.<sup>42</sup>

**Cyclic Voltammetry.** Electrochemical data of compounds **1–7** were obtained in about 1 mmol/L DMF solutions using [*n*-Bu<sub>4</sub>N]PF<sub>6</sub> (0.1 mol/L) as the supporting electrolyte. The CV data of compounds **1–7** are summarized in Table 8. As shown in Supporting Information, Figure S6 in the range –1.5 to +0.6 V (vs SCE), *E*<sub>1/2</sub> of the redox possess associated with A<sup>2-</sup>\A<sup>3-</sup> (A<sup>2-</sup> = anion cluster of compounds **1–7**; A<sup>3-</sup> = reduced anion cluster) are found at –0.762 V for **1**, –1.011 V for **2**, –0.753 V for **3**, –0.771 V for **4**, –0.910 V for **5**, –0.752 V for **6**, and –0.754 V for **7**, respectively. Under the same conditions, the [Bu<sub>4</sub>N]<sub>2</sub>[Mo<sub>6</sub>O<sub>19</sub>] parent shows one redox possesses about –0.494 V (*E*<sub>1/2</sub>), and the large cathodic shift of those compounds suggests that these organoimido derivatives of hexamolybdate are more difficult to be reduced than the [Mo<sub>6</sub>O<sub>19</sub>]<sup>2-</sup> parent, namely, the hexamolybdate cluster in organoimido

(31) Nugent, W.; Mayer, J. E. *Metal-Ligand Multiple Bonds*; Wiley: New York, 1988.

**Table 7.** <sup>1</sup>H-NMR Chemical Shift of Organic Ligand in Compounds 1–7, Corresponding Organic Amine Compounds, and Corresponding Nitro Compounds

Compound	NH <sub>2</sub>	NO <sub>2</sub>	[NMo <sub>6</sub> O <sub>18</sub> ] <sup>2-</sup>	[NMoO <sub>17</sub> (NR)] <sup>2-</sup>
	a 8.36 b 6.485 c 6.426 *400M DMSO-d <sub>6</sub>	a 11.1 b 6.959 c 8.139 *400M DMSO-d <sub>6</sub>	a 10.160 b 6.7838 c 7.1101 300M CD <sub>3</sub> CN-d <sub>3</sub>	a 9.9932 b 6.7598 c 7.0494 300M DMSO-d <sub>6</sub>
	a 8.29 b 6.444 c 6.415 d 6.357 e 1.985 *400M DMSO-d <sub>6</sub>	a 5.50 b 6.75 c 6.75 d 8.050 e 2.615 *90M CDCl <sub>3</sub>	a 10.04 b 6.70 c 6.46 d 7.06 e 2.56 300M DMSO-d <sub>6</sub>	a 9.854 b 6.590 c 6.548 d 6.998 e 2.468 300M DMSO-d <sub>6</sub>
	A 9.7941 b 6.7838 c 7.1604 d 7.3504 e 6.6442 f 7.1066 g 7.4717 300M DMSO-d <sub>6</sub>	-	a 10.4293 b 6.9990 c, f 7.4878 d 7.3825 e 7.9433 g 8.0818 300M DMSO-d <sub>6</sub>	-
	A 3.545 b 2.665 c 1.920 d 1.840 e 1.300 f 1.153 *400M CDCl <sub>3</sub>	-	a 3.5997 b 4.4421 OH 3.7736 c, d 2.0717 e 1.3952 f 1.7375 300M acetone-d <sub>6</sub>	-

\* Spectral Database for Organic compounds (SDBS).

derivatives of hexamolybdate bear more high electron density than the [Mo<sub>6</sub>O<sub>19</sub>]<sup>2-</sup> parent because organoimido ligands possess superior electron-donating ability compared to oxo ligands. The cathodic shift of  $E_{1/2}$  between compounds 1–7 and hexamolybdate parent is 0.268 V for 1, 0.517 V for 2, 0.259 V for 3, 0.277 V for 4, 0.416 V for 5, 0.258 V for 6, and 0.260 V for 7, respectively. It is obvious that bifunctionalized derivatives have more large cathodic shifts than corresponding monofunctionalized derivatives, indicating that bifunctionalized derivatives are in possession of more electron density, as evidenced in structure and NMR study, and are more difficult to be reduced than monofunctionalized derivatives, in accordance with the study of Maatta.<sup>21</sup>

**BVS and DFT Calculations.** Bond valence sum (BVS)<sup>32</sup> for compounds 1–7 are listed in Supporting Information, Table S2, and confirm that all molybdenum atoms in compounds 1–7 are in the +6 oxidation state (values 5.817–6.354). The BVS of the terminal oxo ligands are generally smaller than that of the bridged oxo ligands, suggesting that the former have more remaining valence than the latter.

(32) Brese, N. E.; O'Keeffe, M. *Acta Crystallogr.* **1991**, *B47*, 192.

(33) Frisch, M. J.; Trucks, G. W.; Schlegel, H. B.; Scuseria, G. E.; Robb, M. A.; Cheeseman, Jr. J. R.; Montgomery, J. A.; Vreven, T.; Kudin, K. N.; Burant, J. C.; Millam, J. M.; Iyengar, S. S.; Tomasi, J.; Barone, V.; Mennucci, B.; Cossi, M.; Scalmani, G.; Rega, N.; Petersson, G. A.; Nakatsuji, H.; Hada, M.; Ehara, M.; Toyota, K.; Fukuda, R.; Hasegawa, J.; Ishida, M.; Nakajima, T.; Honda, Y.; Kitao, O.; Nakai, H.; Klee, M.; Li, X.; Knox, J. E.; Hratchian, H. P.; Cross, J. B.; Adamo, C.; Jaramillo, J.; Gomperts, R.; Stratmann, R. E.; Yazyev, O.; Austin, A. J.; Cammi, R.; Pomelli, C.; Ochterski, J. W.; Ayala, P. Y.; Morokuma, K.; Voth, G. A.; Salvador, P.; Dannenberg, J. J.; Zakrzewski, V. G.; Dapprich, S.; Daniels, A. D.; Strain, M. C.; Farkas, O.; Malick, D. K.; Rabuck, A. D.; Raghavachari, K.; Foresman, J. B.; Ortiz, J. V.; Cui, Q.; Baboul, A. G.; Clifford, S.; Cioslowski, J.; Stefanov, B. B.; Liu, G.; Liashenko, A.; Piskorz, P.; Komaromi, I.; Martin, R. L.; Fox, D. J.; Keith, T.; Al-Laham, M. A.; Peng, C. Y.; Nanayakkara, A.; Challacombe, M.; Gill, P. M. W.; Johnson, B.; Chen, W.; Wong, M. W.; Gonzalez, C.; Pople, J. A. *GAUSSIAN 03*, Revision A.1; Gaussian, Inc.: Pittsburgh, PA, 2003.

**Table 8.** Summary of Cyclic Voltammetry Data of Compounds 1–7

compound	$E_{pc}$ , V	$E_{pa}$ , V	$E_{pa} - E_{pc}$ , V	$E_{1/2}$ , V	cathodic shift, V
[Mo <sub>6</sub> O <sub>19</sub> ] <sup>2-</sup>	-0.564	-0.404	0.160	-0.494	0
1	-0.842	-0.681	0.161	-0.762	0.268
2	-1.066	-0.957	0.109	-1.011	0.517
3	-0.817	-0.688	0.129	-0.753	0.259
4	-0.836	-0.707	0.129	-0.771	0.277
5	-0.971	-0.849	0.122	-0.910	0.416
6	-0.823	-0.681	0.142	-0.752	0.258
7	-0.837	-0.670	0.167	-0.754	0.260

To explore the origin of the first excitation and the interaction between the hexamolybdate cluster and ary-limido ligand in compounds 1–6, we had done simulated UV absorption calculations. In this text, all electronic excitation energies were calculated within Gaussian03 program package<sup>33</sup> by employing time dependent density functional theory (TD-DFT) at the gradient-corrected B3LYP level with Becke's three parameter functional<sup>34</sup> and Lee–Yang–Parr functional<sup>35</sup> using the LanL2DZ basis set in which the effective core potential (ECP)<sup>36</sup> was used for the Mo atoms and 6-31G\* for other non metal atoms. The geometries were established according to crystallographic data without geometrical optimization.

Mulliken atom charge analysis for compounds 1–6 (as shown in Supporting Information, Table S3) shows clearly that the Mulliken atom charges of nitrogen atoms of the imido ligand are larger than that of the terminal oxo ligands, in accordance with the fact that the electron-donating ability of the imido ligand are superior than that of the terminal oxo ligands. Correspondingly, the Mulliken atom charges of the imido-bearing molybdenum atoms are smaller than those of other molybdenum atoms; the Mulliken atom charges of terminal oxo ligands are smaller than those of bridged oxo ligands, implying that the electronegativity and basicity of terminal oxo ligands are less than that of bridged oxo ligands, in agreement with the BVS results and calculations on [donor]<sup>+</sup><sub>2</sub>[Mo<sub>6</sub>O<sub>19</sub>] (donor = Me<sub>3</sub>TTF-CH<sub>2</sub>OH, EDT-TTF(CH<sub>2</sub>OH)<sub>2</sub> and TTF(CH<sub>2</sub>OH)<sub>4</sub>),<sup>43</sup> which answers for in part the case that bridged oxo ligands are more inclined to form hydrogen bonding as hydrogen bonding acceptors than terminal oxo ligands.

According to the TD-DFT calculations, the first excitation has no contribution to the calculated oscillator strength for all of the compounds, and so the actual contribution of the first electronic excitation to the UV absorption can be negligible. For all these compounds, the excited states with big oscillator strengths differ from the origins of electron transfers, that is, from POMs to ligand, ligand to POM, or intraligand.

The simulated UV spectra are similar with the observed first UV absorption band (Supporting Information, Table S4). The peak of the simulated UV absorption band appears at 334 nm for 1, 353 nm for 2, 328 nm for 3 and 4, 346.88 nm for 5, and 372 nm for 6, respectively, which are in close to the corresponding experimental values.

(34) Becke, A. D. *J. Chem. Phys.* **1993**, *98*, 5648.(35) Lee, C.; Yang, W.; Parr, R. G. *Phys. Rev. B* **1988**, *37*, 785.

**Study of Optical Band Gap.** To investigate the potential conductivity of these compounds, the measurement of diffuse reflectivity for powder samples of compounds **1–7** was used to obtain their band gap ( $E_g$ ). The  $E_g$  was determined as the intersection point between the energy axis and the line extrapolated from the linear portion of the absorption edge in a plot of the Kubelka–Munk function  $F$  against energy  $E$ . The Kubelka–Munk function,  $F = (1 - R)^2/2R$ , was converted from the recorded diffuse reflectance data, where  $R$  is the reflectance of an infinitely thick layer at a given wavelength.<sup>40</sup> On the  $F$  versus  $E$  plot (Supporting Information, Figure S5) a steep absorption edge is displayed from which the  $E_g$  for compounds **1**, **2**, **3**, **4**, **5**, **6**, and **7** can be assessed at 2.59 eV, 2.59 eV, 2.66 eV, 2.62 eV, 2.61 eV, 2.23 eV, and 2.79 eV. The  $E_g$  of **1–7** are smaller than that of the parent  $(\text{Bu}_4\text{N})_2[\text{Mo}_6\text{O}_{19}]$  ( $E_g = 2.90$  eV), which also indicates the formation of the Mo–N multiple bond. The delocalization of  $\pi$  electrons from the conjugated organoimido ligand to the metal oxygen cluster in compounds **1–6** reduce remarkably the energy level difference between the oxygen  $\pi$ -type highest occupied molecular orbital (HOMO) and the molybdenum  $\pi$ -type lowest unoccupied molecular orbital (LUMO) compared to that of  $[\text{Mo}_6\text{O}_{19}]^{2-}$ . Compound **6** has the smallest band gap owing to the extended delocalization, while compound **7** has the largest band gap owing to the shortness of  $\pi$  electrons in the corresponding organoimido ligand.

(36) (a) Dunning, T. H., Jr.; Hay, P. J. In *Modern Theoretical Chemistry*; Schaefer, H. F., III, Ed.; Plenum: New York, 1976; Vol. 3, pp 1–28. (b) Hay, P. J.; Wadt, W. R. *J. Chem. Phys.* **1985**, *82*, 270.

(37) Nur, N. H.; Klemperer, W. G.; Wang, R. C. *Inorg. Synth.* **1990**, *27*, 78.

(38) (a) Sheldrick, G. M.; *SHELXS-97, Program for solution of crystal structures*; University of Göttingen: Göttingen, Germany, 1997. (b) Sheldrick, G. M.; *SHELXL-97, Program for refinement of crystal structures*; University of Göttingen: Göttingen, Germany, 1997.

(39) Zhu, L.; Zhu, Y. L.; Meng, X. G.; Hao, J.; Li, Q.; Wei, Y. G.; Lin, Y. B. *Chem.—Eur. J.* **2008**, *14*, 10923.

(40) (a) Pankove, J. I. *Optical Processes in Semiconductors*; Prentice-Hall: Englewood Cliffs, NJ, 1971; (b) Wesley, W. M.; Harry, W. G. H. *Reflectance Spectroscopy*; Wiley: New York, 1966.

(41) Li, Q.; Wu, P.; Wei, Y.; Xia, Y.; Wang, Y.; Guo, H. Z. *Anorg. Allg. Chem.* **2005**, *631*, 773.

(42) (a) Li, Q.; Wei, Y.; Hao, J.; Zhu, Y.; Wang, L. *J. Am. Chem. Soc.* **2007**, *129*, 5810. (b) Li, Q.; Wang, L.; Yin, P.; Wei, Y.; Hao, J.; Zhu, Y.; Zhu, L.; Yuan, G. *Dalton Trans.* **2009**, 1172.

(43) Dolbecq, A.; Guirauden, A.; Fourmigué, M.; Boubekur, K.; Batail, P.; Rohmer, M.-M.; Bénard, M.; Coulon, C.; Sallé, M.; Blanchard, P. *J. Chem. Soc., Dalton Trans.* **1999**, 1241.

(44) (a) Qiu, Y.; Xu, L.; Gao, G.; Wang, W.; Li, F. *Inorg. Chim. Acta* **2006**, *359*, 451. (b) Li, Q.; Wu, P.; Wei, Y.; Wang, Y.; Wang, P.; Guo, H. *Inorg. Chem. Commun.* **2004**, *7*, 524. (c) Li, Q.; Wu, P.; Xia, Y.; Wei, Y.; Guo, H. *J. Organomet. Chem.* **2006**, *691*, 1223. (d) Proust, A.; Thouvenot, R.; Chaussade, M.; Robert, F.; Gouzerh, P. *Inorg. Chim. Acta* **1993**, *224*, 81.

## Conclusion

In summary, a series of remote hydroxyl functionalized organoimido derivatives, including  $(\text{Bu}_4\text{N})_2[\text{Mo}_6\text{O}_{18}(\text{Cres})]$  (**1**),  $(\text{Bu}_4\text{N})_2[\text{Mo}_6\text{O}_{17}(\text{Cres})_2] \cdot \text{H}_2\text{O}$  (**2**),  $(\text{Bu}_4\text{N})_2[\text{Mo}_6\text{O}_{18}(\text{Phen})] \cdot i\text{-PrOH}$  (**3**),  $(\text{Bu}_4\text{N})_2[\text{Mo}_6\text{O}_{18}(\text{Phen})] \cdot \text{EtOH}$  (**4**),  $(\text{Bu}_4\text{N})_2[\text{Mo}_6\text{O}_{17}(\text{Phen})_2]$  (**5**),  $(\text{Bu}_4\text{N})_2[\text{Mo}_6\text{O}_{18}(\text{Naph})]$  (**6**), and  $(\text{Bu}_4\text{N})_2[\text{Mo}_6\text{O}_{18}(\text{Chex})] \cdot 2\text{H}_2\text{O}$  (**7**) were prepared and characterized to explore their intermolecular hydrogen bonding interactions and supramolecular assembly. Single crystal X-ray diffraction structural study reveals that their hydrogen bonding supramolecular assembly vary from 0D dimer (**4**), to 1D infinite wavelike single chain (**3**), to 1D infinite double chain (**2**), to 2D network (**1**, **5**, **6**, **7**) because of the alteration of grafting organic ligands, the substituent extent, and solvent molecules. Intermolecular and intramolecular hydrogen bonding not only play an important role in their cell packing and supramolecular assembly but also have an important influence on their anion cluster conformation; the rotatable C–N single bond allows them to stand in different positions with different dihedral angles between the aryl ring plane and the  $\text{Mo}_4\text{O}_4$  plane to accommodate their different hydrogen bonding interactions. DFT calculations show that the bridged oxo ligands have higher electronegativity and charge density compared to the terminal oxo ligand, resulting in bridged oxo ligands that are more inclined to form hydrogen bonding as acceptor than the terminal oxo ligand. After the attachment of the organoimido ligand onto the hexamolybdate cluster, the lowest energy electronic transition in their UV absorption spectra for compound **1–6** shows a large bathochromic shift due to strong d- $\pi$  interaction;  $^1\text{H}$  NMR of aryl hydrogen in compounds **1–6** shows obvious downfield shifts owing to the electron-withdrawing effect of the POMs compared to that of free amine; compounds **1–7** are more difficult to be reduced than the parent  $(\text{TBA})_2[\text{Mo}_6\text{O}_{19}]$ ; solid state diffuse reflectance shows that the grafting of conjugated organic ligand can reduce the optical band gap of hexamolybdates efficiently. Our current researches not only study systematically the hydrogen bonding interaction in remote hydroxyl functionalized organoimido derivatives of POMs and their supramolecular assembly but also provide some available precursors of remote hydroxyl functionalized POMs for further esterification reaction. The relevant study is underway in our laboratory.

**Acknowledgment.** This work is sponsored by NFSC 20871073, THSGZ, and Tsinghua SRT program, CPSF 023260204 and Tsinghua University Postdoctoral Science Foundation (TUPSF, no. 023160204).

**Supporting Information Available:** Additional information as noted in the text. This material is available free of charge via the Internet at <http://pubs.acs.org>.